Research Square

Preprints are preliminary reports that have not undergone peer review.
They should not be considered conclusive, used to inform clinical practice,
or referenced by the media as validated information.

Green Synthesis and Physicochemical Characterization of Zno-Modified Fe_2O_3 Nanoparticles for Environmental Applications

Pradeep Kumar Singh
GLA University
Vinod Kumar Naidu Pamuluri
VinodKumarNaiduPamuluri10@outlook.com
Pragati Engineering College
Seelam Navya Sree
Vardhaman College of Engineering
Vipulsinh Rajput
Gokul Global University
A Saravanan
Aditya University
Ankit Punia
Chitkara University
Bipin Sule
Vishwakarma Institute of Technology
Kapil Mundada
Vishwakarma Institute of Technology
Mahendran Arumugam
Saveetha Medical College, Saveetha Institute of Medical and Technical Sciences

Research Article

Keywords: Environmental Remediation, Heavy Metal Adsorption, Photocatalytic Degradation, Quantum-Inspired Optimization, Wastewater Treatment, Zinc Oxide–Iron Oxide Nanocomposites

Posted Date: July 30th, 2026

DOI: https://doi.org/10.21203/rs.3.rs-10343354/v1

License: This work is licensed under a Creative Commons Attribution 4.0 International License.
Read Full License

Additional Declarations: No competing interests reported.

GREEN SYNTHESIS AND PHYSICOCHEMICAL CHARACTERIZATION OF ZNO-MODIFIED FE_2O_3 NANOPARTICLES FOR ENVIRONMENTAL APPLICATIONS

[1]Pradeep Kumar Singh, [2*]Vinod Kumar Naidu Pamuluri, [3]Seelam Navya Sree, [4]Vipulsinh Rajput, [5]A. Saravanan, [6]Ankit Punia, [7]Bipin Sule, [8]Kapil Mundada, [9]Mahendran Arumugam

[1]Department of Mechanical Engineering, Institute of Engineering and Technology, GLA University Mathura, Uttar Pradesh, India-281406.

[2*]Assistant Professor, Department of Mechanical Engineering, Pragati Engineering College, Surampalem, Kakinada District, Andhra Pradesh, India -533437.

E-mail: VinodKumarNaiduPamuluri10@outlook.com

[3]Assistant Professor, Dept. of Mechanical Engineering, Vardhaman College of Engineering, Shamshabad, Hyderabad, India - 501 218.

[4]Department of Mechanical Engineering, Faculty of Engineering, Gokul Global University, Siddhpur, Gujarat, India.

[5]Department of Mechanical Engineering, Aditya University, Surampalem, Andhra Pradesh, India, Pin 533437

[6]Centre of Research Impact and Outcome, Chitkara University, Rajpura- 140417, Punjab, India

[7]Department of Engineering, Science and Humanities, Vishwakarma Institute of Technology, Pune, Maharashtra, 411037, India

[8]Department of Instrumentation and Control Engineering, Vishwakarma Institute of Technology, Pune, Maharashtra, 411037 India.

[9]Center for Global Health Research, Saveetha Medical College, Saveetha Institute of Medical and Technical Sciences, Chennai, India

Corresponding author

Vinod Kumar Naidu Pamuluri, VinodKumarNaiduPamuluri10@outlook.com

Abstract

Nanotechnology has paved the way for the development of Fe_2O_3 nanoparticles modified by ZnO showing high adsorption capacity and enhanced catalytic activity, which have gained great interest for advanced environmental remediation and photocatalytic treatment of wastewater. The use of intelligent computational tools in the synthesis of nanomaterials further extends pollutant degradation abilities, structural strength and environmental adaptability in varying operational conditions. However, prediction and optimization methods are existing and have poor prediction accuracy, high computational complexity, low convergence stability and low environmental adaptability. To overcome the above constraints, this research presented a Hierarchical Cognitive Neuro Forecasting Framework (HCNFF) and Adaptive Quantum Automation Intelligence Network (AQAI-Net) to realize intelligent prediction of nanoparticles and automatic optimization of the environment. The HCNFF predicted the photocatalytic degradation efficiency and adsorption performance with the hierarchical feature reconstruction and adaptive neural forecasting and cognitive learning mechanisms. Simultaneously, AQAI-Net implemented quantum-inspired optimization, adaptive learning and automatic control regulation for optimization of synthesis parameters. Experimental results showed that the system performance was better with a maximum prediction accuracy of 98.88% and optimization accuracy of 98.91% respectively. The general proposed

framework was found to be very useful to propose a scalable and reliable solution for the sustainable environmental nanotechnology applications.

Keywords: Environmental Remediation, Heavy Metal Adsorption, Photocatalytic Degradation, Quantum-Inspired Optimization, Wastewater Treatment, Zinc Oxide–Iron Oxide Nanocomposites

1. Introduction

The metal oxide based nano photocatalysts such as ZnO and Fe_2O_3 based nanocomposites, have been widely studied in the field of environmental remediation applications owing to their high efficiency. More recently, bio-inspired and green synthesis techniques have been proven to enhance the photocatalytic activity of the α-Fe2O3/ZnO nanobinary system for the degradation of anionic and cationic dyes while maintaining excellent reusability features of the nanobinary system (Bouafia et al., 2025). The chemically synthesized ZnO/Fe_2O_3 Nanocomposites also exhibited impressive performance to degrade mixed dye pollutants which indicated its potential for wastewater treatment system (Manojkumar et al., 2024). A series of other interesting hybrid structures such as the ZnO@Fe_2O_3-Ag/AgCl has been grown to enhance the magnetic separation and photocatalytic performance (Asghari et al., 2025). Similarly, it has been shown that the degradation efficiency of Fe_3O_4 doped ZnO nanostructures synthesized by Pulsed Laser Ablation (PLA) is increased with the influence of structural engineering for the performance of the catalyst (Al-Essa et al., 2025). Green synthesis routes with plant extracts have also allowed for the development of multiple functional ZnO/Fe_2O_3 nanocomposites with photocatalytic, antibacterial and antioxidant capabilities (Bollinger et al., 2026). Moreover, it has been reported that the doping and co-precipitation techniques can drastically affect the structural and optical properties of the Zn doped α-Fe_2O_3 nanoparticles, which can make them more useful for environmental applications (Green et al., 2024).

Some other applications are also developed using these nanomaterials, such as biofertiliser in agriculture (Akbar et al., 2024) and, the combination of ZnO, Fe2O3 systems is still showing promising multifunctional applications for both photocatalysis and electronic device applications (Racik et al., 2024). They have also been proved to be effective for removing hydrocarbons and heavy metals from contaminated water by employing mixed metal oxide systems (Gherbi et al., 2024) and magnetic materials such as Fe_3O_4, ZnO composites for removing organic dyes such as Rhodamine B in photocatalytic degradation (Qi et al., 2024) were found to be excellent. Apart from photocatalytic property, green synthesized ZnO nanoparticles exhibit excellent antibacterial activity, antifungal activity and antioxidant activity which are attributed to the phytochemical modification process (Haiouani et al., 2024) and also due to use of plant-based synthesis methods such as Verbascum sinaiticum extract (Tigabu et al., 2025) that further increases the antimicrobial property of ZnO nanoparticles. Advanced composite material such as Fe_3O_4 SiO_2 ZnO activated with H_2O_2 has been shown to have good ability to degrade azo dyes with UV light (Makota et al., 2024). The field of photocatalytic studies is increasingly being explored using Machine Learning (ML) to increase the accuracy

of predictions and optimize degradation processes, particularly those involving removal of pesticides from water using ZnO based photocatalytic systems (Song et al., 2024). Furthermore, experimental validation works of photocatalysts such as Cu_2O/WO_3 and ZnO coupled with machine learning models have shown improvements in performance and prediction in environmental remediation applications (Nawaz et al., 2025). All these developments are a testament to the shift from conventional photocatalytic systems to "smart" approaches to nanomaterials design for sustainable environmental applications based on data. In this research provides a contribution such as:

- A Hierarchical Cognitive Neuro Forecasting Framework (HCNFF) for accurate multi-level prediction of photocatalytic degradation efficiency, adsorption capacity and structural stability of ZnO-doped Fe_2O_3 nanoparticles is proposed by the research, which makes use of hierarchical feature reconstruction and adaptive neural learning.
- It provide a cognitive feature adaptation process, which aims to select the most significant features of the synthesis with an intelligent feature selection mechanism, such as the concentration of doping agents of ZnO; calcinations temperature; pH conditions and ratio of the precursors; and quantifies them to increase the interpretability and reliability of the model.
- An effective optimization and automation strategy using Adaptive Quantum Automation Intelligence Network (AQAI-Net) for optimizing synthesis condition and environmental performance of nanoparticles is developed, which is based on quantum-inspired probabilistic search, adaptive learning and automated control.
- Advanced deep learning, evolutionary optimization and quantum-inspired computation are combined in the proposed framework to boost convergence speed, decrease computational complexity and improve real-time adaptability to the environment in dynamic operating conditions.
- The HCNFF and AQAI-Net system are high accuracy, stable and scalable in photocatalytic wastewater treatment and heavy metal removal system which is suitable to use in environmental nanotechnology applications.

The main objective of this research is to present the proposed framework for developing ZnO doped Fe_2O_3 nanoparticles for environmental applications in a systematic manner. The section 2 of the work is a background study, where existing ML and optimization techniques and their shortcomings and research gaps. In Section 3, the proposed HCNFF and AQAI-Net is described, as well as details on the datasets and methodology. Experimental setup and result are described in Section 4, performance analysis, comparisons; ablation study and validation are discussed in Section 5. Finally, Section 6 summarizes the results and directions for future work.

2. Background Study

Recently, (Yılmaz et al., 2024) proposed a morphological analysis framework using deep learning and attention mechanism to extract features from the SEM image, which improves the feature extraction process. However, the research is mainly based on the advanced CNN-based vision modeling, which has several drawbacks, including reliance on the data sets and high computational demands. One of the gaps in the research is the extension of such deep learning methods for multi-material nanocomposites and further studies into more general applications in photocatalysis.

To accurately recognize the structure and size of nanoparticles from electron microscopy image data, (Ju et al. 2025) have proposed a novel CNN model. While it can be very effective in improving the capabilities of nanostructure analysis, it would not be possible in the generalisation of model in other imaging systems to be successful. The limitation is that information derived from multi-modal images is not used.

(Arenas et al., 2025)have developed machine learning models such as Bagging, Extra Trees and Random Forest to predict the band gap energy (BGE) of high entropy (HE) oxides using their UV-Vis spectroscopy data. The method is helpful for increase the prediction accuracy, however, it has a few disadvantages; it requires feature engineering and it is not easy to interpret. Lack of physics-informed ML model with enhanced explainability.

The prediction of band gap in low-symmetry perovskites was done by Alsaedi et al. 2024 [19] using the algorithm of SVR, RFR, GBR and XGBoost. The study has good predictive accuracy and limited data and experimental validation. The need for hybrid deep learning frameworks with incorporation of domain knowledge is the gap.

(Feng et al. 2024)used multiple ML models including XGBoost, RF, LightGBM and GBR to model the band gap of hybrid perovskites. Results indicate high accuracy, but there are problems of model overfitting and lack of real-world validation. It is found that there is a gap in the research that generalized models can be developed in various material systems.

(Sheikhmohammadi et al., 2024) used machine learning approach for the optimization of the WO_3/Co-ZIF nanocomposite toward the removal of cefixime. The method has good adsorption prediction performance, but has a small range of applications and is not balanced. The use of ML models to multi-pollutant wastewater systems is increasing the gap.

To design nanostructured metal oxide photoanodes for water splitting applications, (Liang et al., 2025)proposed machine learning based CNN approaches. The approach improves efficiency in material discovery tasks yet has constraints with regards to the size of training data and the computational complexity. A paucity of research exists for real-time adaptive ML-guided synthesis systems.

(Kakhki et al., 2025) optimized photocatalytic degradation of tetracycline by S-doped ZnO/chitosan composites by using Random Forest Regression. The model is good for optimization of parameters but is

not transferable to other photocatalysts. Multi-model ensemble learning, for more robust systems, is lacking.

Table 1: Comparative Analysis of Computational Optimization Techniques in Nanomaterial and Photocatalytic Research

Author	Model / Method	Concept	Technique Used	Key Limitation	Research Gap
Sheikhmohammadi et al. (2025)	Gradient Boosting Regression	Photocatalytic degradation optimization of tetracycline using UV/ZrO_2/NaOCl system	Supervised ML regression (GBR) for reaction pathway optimization	Limited generalization to other pollutants and systems	Need multi-pollutant adaptable ML frameworks
Zainulabdeen et al. (2025)	LSTM Network	Prediction of antibacterial activity of nanoparticles	Multi-branch LSTM with SHAP explainability	High computational cost and data dependency	Lack of scalable real-time prediction models
Rehman et al. (2025)	Genetic Algorithm (GA)	AI-guided optimization for photocatalysis wastewater treatment	Evolutionary optimization with supervised ML integration	Convergence may be slow for large datasets	Need hybrid GA–deep learning hybrid systems
Konstantopoulos et al. (2022)	Particle Swarm Optimization (PSO)	Nanomaterial manufacturing optimization with ML strategies	Swarm intelligence-based optimization	Susceptible to local minima	Need adaptive PSO with hybrid global search enhancement
Khamkure et al. (2026)	Fuzzy Logic Optimization	Magnetic biochar nanocomposite synthesis for arsenic removal	Fuzzy-driven optimization (MiFREN model)	Limited precision in highly nonlinear systems	Need integration with ML-based predictive control

Zhu et al. (2025)	Artificial Neural Network (ANN / ANFIS)	Biodiesel optimization and emission prediction	ANN + ANFIS hybrid modeling	Black-box nature reduces interpretability	Need explainable AI-based hybrid nanomaterial models
Halawa et al. (2026)	Quantum-Inspired Optimization	Nanophotonics and energy applications optimization	Quantum-inspired heuristic optimization	High complexity and computational overhead	Need lightweight quantum-ML hybrid frameworks

Table 1 summarizes the recent methods of optimization and machine learning using artificial intelligence that have been used to research nanomaterials and photocatalysis/environmental remediation. The model is fully detailed in each work and is shown how the model improves the accuracy of prediction and the optimization of the process in various applications such as Gradient Boosting Regression, LSTM, Genetic Algorithm, PSO, Fuzzy Logic, ANN and Quantum-Inspired Optimization. There are several existing approaches that have limitations such as high computational cost, lack of generalization, slow convergence and limited interpretability; a more scalable, hybrid and explainable AI framework to facilitate real-time, multi-system environmental applications is yet to be researched and designed.

2.1 Research Gap

The literature reviewed covers several research areas that should be studied to optimize the use of nanomaterials and the photocatalytic treatment. These include the lack of generality of existing models with different pollutant systems, high computational complexity, poor scalability and lack of real-time adaptability and interpretability of existing machine learning and optimization methods. Most of the existing methods are, however, single-model based methods that are not robust enough and applicable to multi-variable environmental systems, which consider complex nonlinear interactions. For these limitations, the proposed HCNFF and AQAI-Net architectures combine the hierarchical cognitive feature learning, adaptive neural forecasting and quantum-inspired optimization strategies in a holistic framework. This hybrid approach greatly improves the prediction accuracy, efficiency of convergence and stability of the system, whilst also decreasing computational load. In this regard the proposed method is an intelligent approach in the context of advanced application of nanomaterials in the environment and provides an explanation and scalability.

3. Proposed Methodology

The proposed intelligent framework to predict the environmental performance of ZnO:Fe_2O_3 nanoparticles and optimize it is presented in this section. Combine a set of benchmark nanomaterials with powerful

computational models to deal with the complex nonlinear relationships in photocatalytic systems. The methodology is organized in HCNFF for prediction of performance and in AQAI-Net for optimization and auto-control of synthesis. The models can be used to scalable and efficient analyse the environmental impacts of nanotechnology with accurate, effective and efficient.

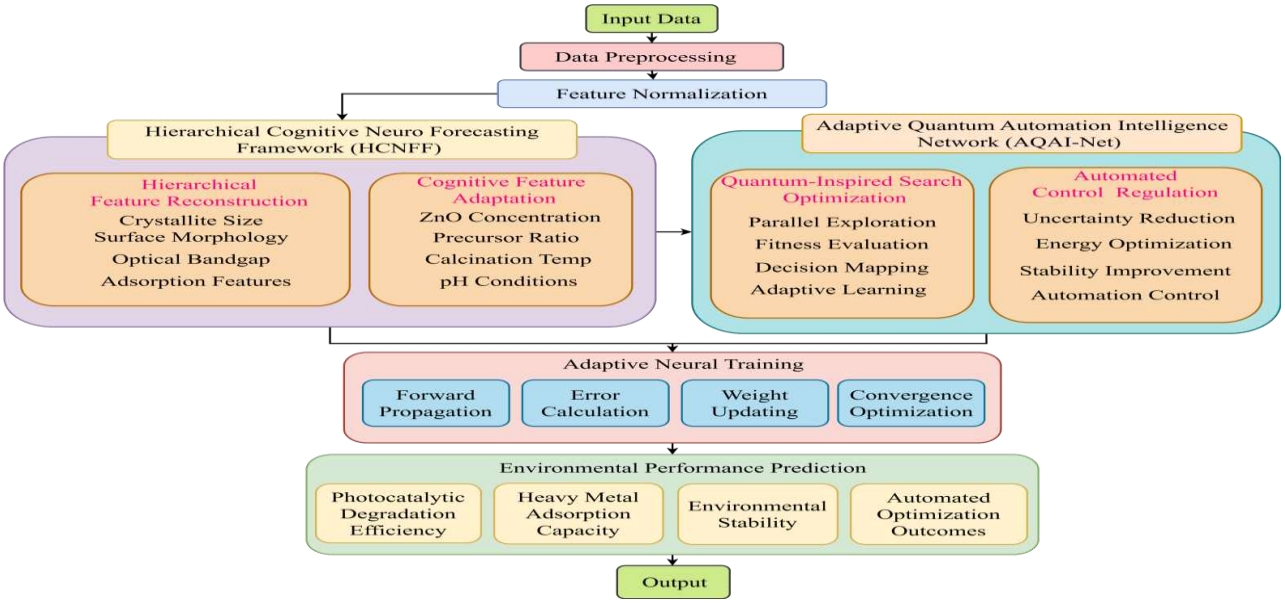


Figure 1: Zno Doped Fe2o3 Nanoparticles for Environmental Applications Architecture

Figure 1 displays the general scheme of the intelligent algorithm proposed that combines the HCNFF and AQAI-Net for environmental nanotechnology uses. The beginning of the process in the proposed algorithm is pre-processing the input data with the nanoparticles and then features normalization in order to improve the consistency of the calculation and the effectiveness of learning. For the purpose of reconstructing the features hierarchically and for adaptation of cognitive features in order to receive the best prediction of the environmental performance of the materials, we use the HCNFF module. Also, for carrying out an optimization of the features in order to obtain the optimal conditions of synthesis and improve the efficiency of automatic regulation, we use the AQAI-Net module. As a result, an accurate prediction of the efficiency of photocatalytic degradation, the capacity for heavy metal adsorption, environmental stability and results of automatic environmental optimization is received.

3.1 Dataset Discription

These researches utilize the dataset of nanomaterials for photocatalysis and wastewater treatment was the one used for information about the materials used in the environment. This data set contains information regarding experiments carried out on synthesised metal oxide nanoparticles such as ZnO, Fe_2O_3, ZnO doped Fe_2O_3, the experimental conditions for the synthesis of the same and their performance in the environment. Concentration of ZnO doping, ratio of precursor, calcination temperature, reaction time, pH, crystallite size and surface area are the main input parameters for this dataset and the main output parameters are the

efficiency of the photodegradation and the adsorption/stability parameters. The dataset has been normalized and de-noised for more consistent and stable dataset to train the model.

3.2 Hierarchical Cognitive Neuro Forecasting Framework (HCNFF)

This research is proposed HCNFF, to accurately predict the environmental performance and behaviour of the ZnO doped Fe_2O_3 nanoparticles. Usually, the predictive model is complex and difficult to apply in complex non-linear relationships between the synthesis parameters and efficiency of the nanoparticles. Based on the above pros and cons, it is proposed to embed the above three mechanisms in an intelligent prediction system HCNFF model. The hierarchical structure allows interesting properties of nanoparticles, like crystallite size, surface morphology, optical bandgap, adsorption capacity and efficiency in the photocatalytic degradation at different levels. Concurrently, the most influential synthesis parameters, like the concentration of ZnO doping, the ratio of the precursor, calcination temperature and the pH conditions, are detected by the cognitive learning layer. The output responses of the environment to the input synthesis parameters are then used to form adaptive nonlinear relationships by deep neural learning techniques in the module of neuro-forecasting.

The approach of HCNFF involves data pre-processing, feature normalization, hierarchical feature reconstruction, adaptive neural training and iterative error optimization. HCNFF methodology includes data pre-processing, feature normalization, hierarchical feature reconstruction, adaptive neural training and iterative error optimization, with the goal of enhancing the accuracy of prediction results and ensuring computational stability. Advanced methods such as intelligent pattern recognition, adaptive weight updating and convergence based learning are incorporated, to reduce the uncertainty in prediction and enhance the reliability of models. This is an iterative process in which it learns from experimental data on nanoparticles to provide optimized prediction of the efficiency of pollutant degradation, the adsorption performance of the pollutant and the stability in the environment. Moreover, HCNFF is able to tackle real-time environmental issues due to its low experimental expenses, less material waste and quick predictions at different working conditions. Standardization of the procedure for the determination of the parameters, training/validation process and optimization steps makes the proposed framework reproducible and hence results in reproducible and stable prediction scenarios for the model using different sets of experimental data and various environmental scenarios. Therefore, HCNFF provides an intelligent forecasting system in the advanced field of environmental nanotechnology, which is efficient, scalable and high performance.

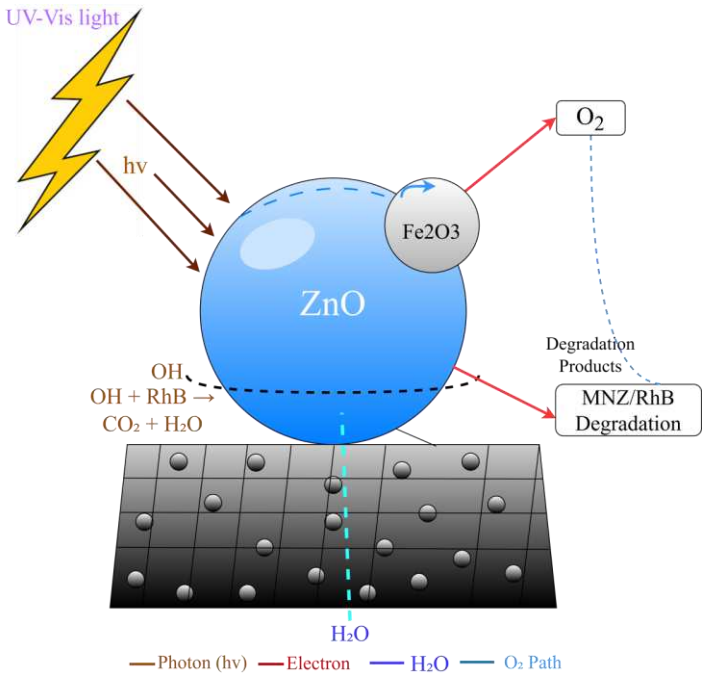


Figure 2: Photocatalytic Degradation Mechanism of ZnO/Fe_2O_3 Nanocomposite under UV–Visible Light Irradiation

The photocatalytic degradation process of the ZnO/Fe_2O_3 nano composite material through UV-Visible light illumination is shown in Figure 2. When illuminated by the UV–visible light, ZnO surface absorbs electrons that transfer to the either of Fe_2O_3 or ZnO materials and generate Reactive Oxygen Species (ROS) such as hydroxyl radicals (•OH) and oxygen radicals. Such ROS reacts with a pollutant molecule such as RhB/MNZ, resulting in the production of benign molecules like CO_2 and H_2O. The Fe_2O_3 part will increase the rate of separation of charges and minimize the recombination of electrons and holes.

$$D = \{(X_i, Y_i)\}_{i=1}^{N} \tag{1}$$

This equation (1) shows the nanoparticles experimental data set is denoted as D and N is the number of samples. X_i Denotes the input synthesis parameter of the ith sample and Y_i is the output response from the environment to the ith sample. In the case of intelligent forecasting and optimization, the variable i takes on the value of an index of the experimental observations.

$$X_{norm} = \frac{X - X_{min}}{X_{max} - X_{min}} \tag{2}$$

This equation (2) is used to normalize synthesis parameters to a common range by carrying out a Min-Max operation. Here, X stands for the value of the feature, X_{min} represents feature's minimum value and X_{max}

represents feature's maximum value. Normalized value of X is calledX_{norm}, which is stable for calculation and is more efficient to be learned by neural networks.

$$H^{(l)} = f(W^{(l)}H^{(l-1)} + b^{(l)}) \tag{3}$$

The equation (3) is based on HCNFF, which is the hierarchical feature extraction. $H^{(l)}$ are the features that are reconstructed at level l and $H^{(l-1)}$ are the features of the previous level. The parameters used are$W^{(l)}$, $b^{(l)}$ and $f(\cdot)$which represent the weight matrix, bias vector and activation function, respectively.

$$C_j = \frac{w_j x_j}{\sum_{k=1}^{m} w_k x_k} \tag{4}$$

This equation (4) shows the score of cognitive importance of synthesis parameters. For this, the value of C_j can be interpreted as the weight of the importance of feature$j$; w_j and x_j are the adaptive weight and feature value, respectively. The denominator is a sum of all the features of the synthesis of$m$, represented by the index k, with their importance.

$$w_j^{new} = w_j^{old} + \eta \frac{\partial E}{\partial w_j} \tag{5}$$

In this equation (5) the weights of the neural features are updated for adaptive learning. The updated weight of j^{th} feature is w_j^{new} and the previous weight isw_j^{old}, respectively and η denotes learning rate, $\frac{\partial E}{\partial w_j}$ is the error gradient with respect to the weight.

$$Z = \sum_{i=1}^{n} W_i X_i + b \tag{6}$$

In equation (6) the neural input that is used for computing the environmental forecast is the weighted. Here, Z is the input vector to the neurons and W_i is the weight of the neuron i and X_i is the normalized input feature for the i^{th} neuron. The variable b is called the bias term and n is representing the number of all input features.

$$f(Z) = \frac{1}{1+e^{-Z}} \tag{7}$$

This equation (7) is known as the sigmoid activation function and is the forecasting network. In this case, the $f(Z)$ is the activation value output of the neurons and the Z is the weighted input to the neurons, where e is an exponential mathematical constant that will change the response of the neurons to be nonlinear.

$$\hat{Y} = f(\sum_{i=1}^{n} W_i X_i + b) \quad (8)$$

The equation (8) shows the environmental response being predicted in HCNFF. W_iIs the weights of the neural network, normalized features and b is the bias term and $\hat{Y}$ is the predicted output. The activation function $f(\cdot)$ is used to transform the synthesis parameters so as to obtain nonlinear prediction output X_i denotes the i^{th} input feature or data value given to the model.

$$E = Y - \hat{Y} \quad (9)$$

This equation (9) gives the forecasting error of this process of neural learning. Prediction error, E and the experimental result of the environment, Y, are variables. $\hat{Y}$ is a variable that indicates the output predicted by HCNFF.

$$MSE = \frac{1}{N}\sum_{i=1}^{N}\left(Y_i - \hat{Y}_i\right)^2 \quad (10)$$

Equation (10) is the optimized in which is a measure of accuracy of the model and is known as Mean Squared Error. In this case, the average squared prediction error for all N samples is called the mean squared error (MSE). Y_i Is the actual output of i^{th} sample and $\hat{Y}_i$ is the predicted output of the i^{th} sample.

$$\theta_{t+1} = \theta_t - \eta \nabla \mathrm{E}(\theta_t) \quad (11)$$

This equation (11) shows the parameters are optimized using adaptive gradient optimization (AGO). The parameter vectors at time t and $t+1$ are denoted as θ_t and θ_{t+1} respectively. The parameter is the step size and the gradient of the prediction error at iteration is denoted as$\eta \nabla \mathrm{E}(\theta_t)$.

$$|E_t - E_{t-1}| < \epsilon \quad (12)$$

This equation (12) shows stopping criterion of neural training. In this instance the prediction errors are E_t and E_{t-1}, at the current and previous iterations respectively. This is the parameter ϵ, threshold for convergence and parameter defining the computational stability.

$$P_d = \frac{C_0 - C_t}{C_0} \times 100 \quad (13)$$

This equation (13) is used to calculate the efficiency of the photo catalytic degradation of nanoparticles. Here, P_d is the percentage of degradation and C_0 is the initial concentration of the pollutant and C_t is the final concentration of the pollutant. The degradation ratio can be given as a percentage, which can be multiplied by 100.

$$Q_e = \frac{(C_i - C_e)V}{m} \tag{14}$$

This equation (14) used to calculate the adsorption capacity of nanoparticles. The pollutant in the system is called C_i and C_e is the concentration of pollutant when the system is at equilibrium; here Q_e is the maximum amount of pollutant that can be adsorbed when the system is at equilibrium. V And m (Mass of the adsorbent) are the parameters of the solution volume and the adsorbent mass.

$$F_{HCNFF} = argmin\left(E_{prediction} + E_{uncertainty}\right) \tag{15}$$

This equation (15) is the last optimization objective of HCNFF. In this case, $argmin$ proposes the set of parameters that minimizes the error: the optimized forecasting function F_{HCNFF}. $E_{prediction}$ Is the prediction error, $E_{uncertainty}$ is the computational uncertainty.

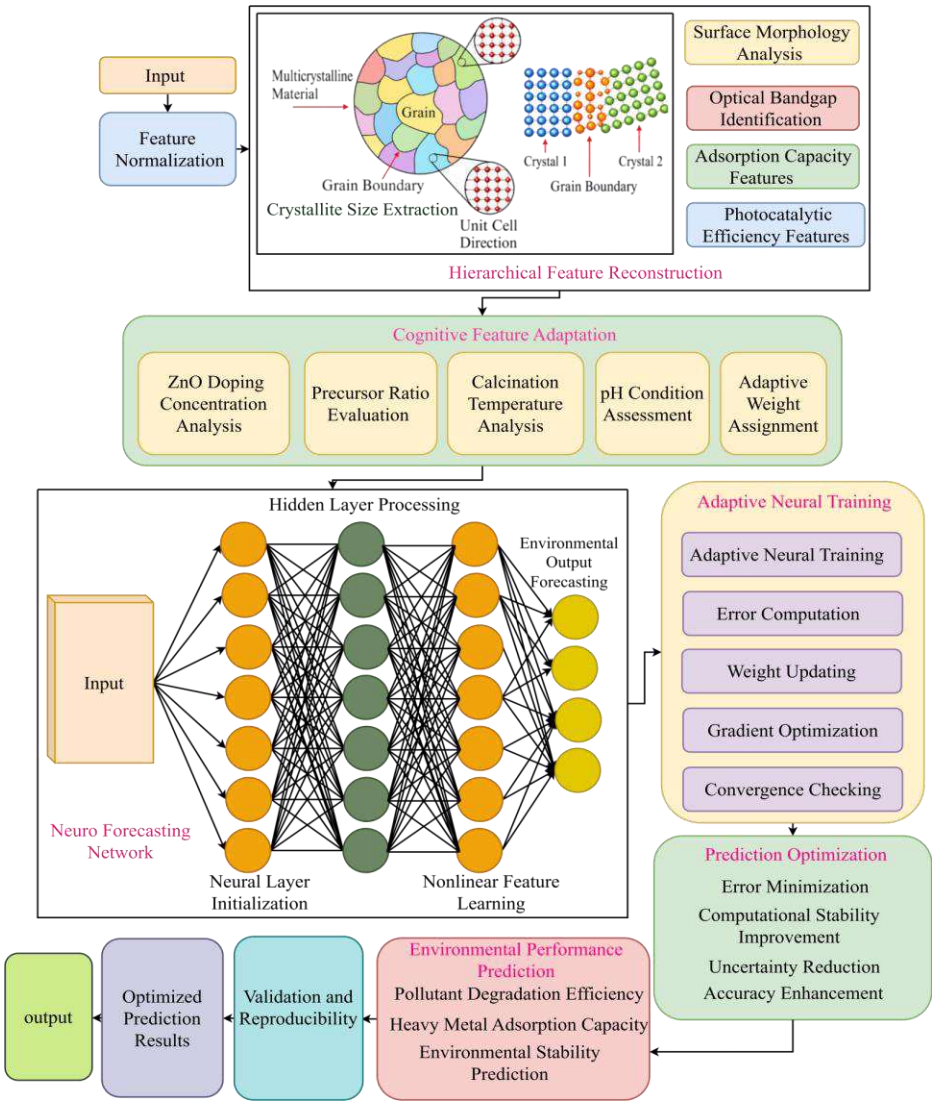


Figure 3: HCNFF workflow

The designed HCNFF for the prediction of environmental performance of Fe2O3 nanoparticles doped with ZnO is shown in Figure 3. The first step involves the preprocessing of experimental data through normalization and hierarchical reconstruction for the extraction of relevant characteristics of nanoparticles, such as particle size, optical energy bandgap, pollutant absorption rate and photodegradation performance. Second, relevant synthesis factors are identified using cognitive feature adaptation and the forecasting neuro network optimally adapts the neural network parameter based on prediction accuracy and numerical computation stability. Finally, it enables the precise prediction of environmental performance, including the degradation efficiency of pollutants and heavy metal adsorption rate.

Algorithm: Hierarchical Cognitive Neuro Forecasting Framework (HCNFF)

Input: Experimental dataset D containing synthesis and environmental parameters
Output: Predicted environmental performance of ZnO-doped Fe_2O_3 nanoparticles
Begin
Step 1: Load Dataset
  Read nanoparticle synthesis dataset D
  Extract input features Xi and output responses Yi
Step 2: Data Preprocessing
  Remove missing and noisy values
  Handle redundant attributes
  Transform categorical values into numerical form
Step 3: Feature Normalization
  Normalize all feature values using Min-Max normalization
    Xnorm = (X - Xmin) / (Xmax - Xmin)
Step 4: Hierarchical Feature Reconstruction
  Divide features into multiple hierarchical levels
  Extract important nanoparticle characteristics:
    - Crystallite size
    - Surface morphology
    - Optical bandgap
    - Adsorption efficiency
    - Photocatalytic degradation rate
Step 5: Cognitive Feature Adaptation
  Analyze synthesis parameters
  Identify influential features using cognitive learning:
    - ZnO doping concentration
    - Precursor ratio
    - Calcination temperature
    - pH conditions
  Assign adaptive feature weights
Step 6: Neuro Forecasting Module
  Initialize neural forecasting network
  Feed reconstructed hierarchical features into network
  Compute nonlinear relationships between inputs and outputs
Step 7: Adaptive Neural Training
  Perform forward propagation
  Calculate prediction error
    Error = Actual Output - Predicted Output

```
    Update network weights using adaptive learning
    Repeat training until convergence criteria are satisfied
Step 8: Prediction Optimization
    Apply iterative error minimization
    Reduce computational uncertainty
    Improve forecasting stability and accuracy
Step 9: Environmental Performance Prediction
    Predict:
        - Pollutant degradation efficiency
        - Heavy metal adsorption capability
        - Environmental stability
Step 10: Validation and Reproducibility
    Perform training-validation testing
    Compare predicted and actual outputs
    Store optimized parameters for reproducible prediction
End
Return optimized environmental prediction results
```

The pseudocode HCNFF functions in the following way: it first preprocesses and normalizes the dataset of nanoparticles so that they are processed in a computational consistent way and irregularities in the data are minimized. Then, the hierarchical feature reconstruction and cognitive feature adaption steps are performed, with which the key synthesis parameters and environmental parameters affecting the performance of the nanoparticles are recovered. Then, Neuro-forecasting module learns the relationship between the output and input variables by adaptive neural method and iterative error optimization to obtain accurate forecast, in a non-linear relationship. Finally, the framework offers a stable, scalable and reproducible prediction of environmental performance for a variety of experimental conditions.

3.3 Adaptive Quantum Automation Intelligence Network (AQAI-Net)

For this research, the synthesis and use of Fe_2O_3 nanoparticles with ZnO doping for use in the environment is proposed, optimizing them intelligently and controlling them automatically through the AQAI-Net. Some real issues that arise in synthesis optimization are multidimensionality of the synthesis variables, nonlinear interactions between the environment and the process and the need for “real time” adaptability of the process. To solve these issues, AQAI-Net is an integrated computational method, which has adaptive optimization; quantum inspired probabilistic search techniques and automated intelligence learning. The main purpose of the framework is to understand the optimum synthesis configuration by analyzing the various parameters of the synthesis such as the concentration of the ZnO doping, the ratio of precursor materials, the calcinations temperature, the duration of the reaction and the pH conditions. AQAI-Net methodology consists of automatic data handling, adaptive parameter optimization, intelligent decision mapping, adaptive fitness evaluation and self-adaptive automation control to improve the efficiency of optimization and computational convergence. To minimize uncertainty in the processing and enhance the reliability of the system, advanced techniques like adaptive weight optimisation, parallel search exploration, convergence based learning and automatic response control are also integrated.

AQAI-Net is still working on experimental data sets of nanoparticles and adapts optimization paths dynamically to generate high performance environmental prediction / automation results. The framework automatically identifies the best operating conditions to maximize the efficiency of photocatalytic degradation, adsorption capacity, stability of the material and response characteristics to the environment. With regard to real-time applications, AQAI-Net can significantly decrease the amount of human interaction, energy usage, experimental costs and speed up automated optimization processes, while changing environmental conditions. Moreover, the proposed framework enables the repeatability of the framework by optimizing the initial values of the parameters, iterative training and validation, repeatable automation phases and convergence mechanisms of the parameters, which ultimately guarantees stable and predictable framework optimization performance for different experimental data sets and scenarios. Therefore, AQAI-Net offers an intelligent, scalable and high-performance optimization and automation system for the advanced environmental nanotech applications.

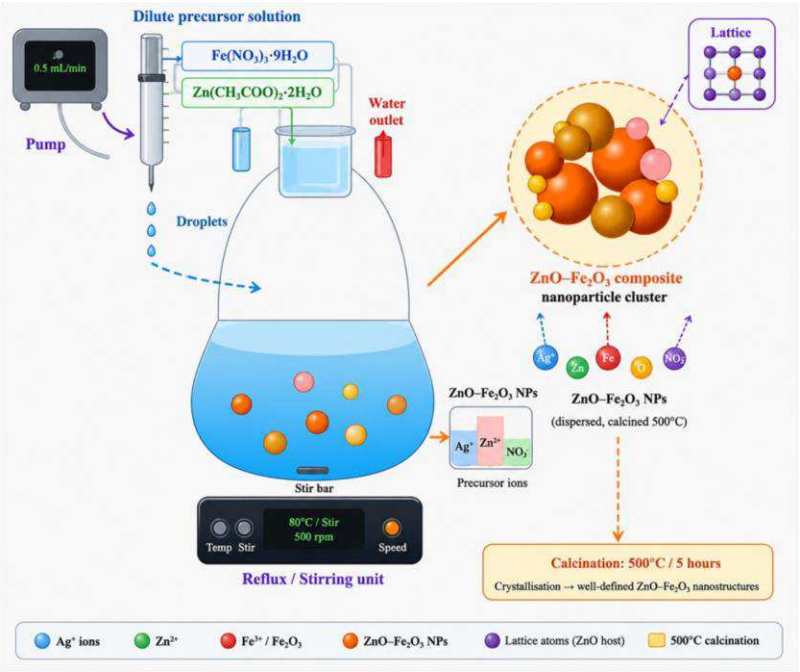


Figure4: Sol–Gel Synthesis of ZnO-Doped Fe_2O_3 Nanoparticles

Figure 4 shows the synthesis procedure of ZnO-Fe_2O_3 composite nanoparticles via a process that involves the refluxing and stirring of chemicals. In this process, the precursors of Fe $(NO_3)_3$•$9H_2O$ and $Zn(CH_3COO)_2$•$2H_2O$ solutions are introduced to the reaction flask by controlled droplets while the reaction is carried out at heating and constant stirring conditions. The resulting nanoparticles are finally calcined at 500°C for 5 hours to obtain perfectly structured ZnO-Fe_2O_3 nanomaterials with enhanced crystallinity and lattice formation.

$$W_i^0 = \frac{1}{n}\sum_{j=1}^{n} X_{ij} \tag{16}$$

The equation (16) used to calculate the adaptive weight for optimization learning at the beginning is calculated. In this instance W_i^0 is the initial weight of the i^{th} optimization parameter and X_{ij} is the value of the jth synthesis feature. n Denotes a number of all the synthesis parameters taken into account during their initialisation.

$$Q_i = \alpha_i|0\rangle + \beta_i|1\rangle \tag{17}$$

This equation (17) is the current state of the art in quantum inspired optimization of AQAI-Net. In this case, α_i and β_i are the probability amplitudes and Q_i is the probabilistic state of the i^{th} optimization solution. For parallel optimization exploration, quantum Inspired Binary uses states: $0\rangle$ and$1\rangle$.

$$|\alpha_i|^2 + |\beta_i|^2 = 1 \tag{18}$$

This equation (18) shows the probability normalization constraint is the quantum-inspired states. Here $|\alpha_i|^2$ and $|\beta_i|^2$are the probabilities for the state's 0 and 1, respectively. They are restricted to the unit interval [0, 1] to make their overall probability 1 so as to be stable probabilistic optimizers.

$$S = \{Q_1, Q_2, Q_3, \dots, Q_n\} \tag{19}$$

The equation (19) describes the number of optimized states explored at the same time. S is the size of the search space and $Q_1, Q_2, Q_3, \dots, Q_n$ is each single quantum inspired optimization state. n is the number of candidate optimization solutions.

$$F_i = \frac{1}{1+E_i} \tag{20}$$

This equation (20) shows the fitness score is computed for each state in optimization, In this case, the fitness value F_i of the ith solution is the optimization error E_i of the i^{th} solution. With efficient optimisation selection, its fitness will be greater as low error will cause low error.

$$E_i = |Y_i - \hat{Y}_i| \tag{21}$$

This equation (21) determines the optimization error. Y_i, $\hat{Y}_i$ are the environmental output, prediction respectively and E_i is the absolute prediction error. The absolute operator || was used to calculate the size of the prediction error.

$$D_{opt} = argmax(F_i) \tag{22}$$

This equation (22) represents an optimum synthesis decision pathway. In this, the optimal decision configuration D_{opt} is optimal choice of decision configuration selected by AQAI-Net. $argmax$ is a function to determine the state x which has the best fitness function F_i .

$$W_i^{new} = W_i^{old} + \eta \Delta W_i \tag{23}$$

This equation (23) the optimization weights are updated adaptively as a result of learning. In this instance, W_i^{new} and W_i^{old} represents the new and old weights, respectively. Parameter η is called the learning rate and the value of ΔW_i is the weight change value during optimization.

$$|F_{t+1} - F_t| < \epsilon \tag{24}$$

This equation (24) gives the convergence criterion of optimization learning. The iterative optimization is terminated when the fitness function value at t^{th} iteration,F_t and $t + 1^{th}$ iteration,F_{t+1} are sufficiently close.

$$R_t = R_{t-1} + \lambda(O_t - R_{t-1}) \tag{25}$$

The equation (25) is used to made the the automated optimization response. In this case, R_t is the regulated response at time$t$ and R_{t-1} is the response at time$t-1$. The regulation factor is λ and O_t is the optimized output at time$t$.

$$U = \frac{1}{N}\sum_{i=1}^{N}(Y_i - \hat{Y}_i)^2 \tag{26}$$

The equation (26) measures the uncertainty in a computation in terms of the mean square prediction error (m.s.p.e.). Here, U is the uncertainty value and Y_i represents the actual output and $\hat{Y}_i$ represents the predicted output. The number of experimental samples denoted as$N$.

$$E_c = \sum_{i=1}^{n} P_i t_i \tag{27}$$

This equation (27) sums up the total energy consumption. In this case, E_c is the total amount of energy consumed and P_i is the energy consumption of the ith operation. The operation takes a variable amount of timet_i.

$$S_t = \frac{1}{1+\sigma^2} \tag{28}$$

This equation (28) is used to measure the stability of AQAI-Net. In the present example, S_t is the stability of the system at iteration t and the dispersion of the result of the optimization are represented byσ^2 the lower the variance, the greater the stability and consistency of the system in automation.

$$AQAI_{opt} = \arg\min(E_{opt} + U + E_c) \tag{29}$$

This equation (29), the last optimization objective of AQAI-Net is presented In this case, $AQAI_{opt}$ denotes the result of optimization of the optimal automation intelligence function. The optimization error, computational uncertainty and the total energy consumption minimized during Adaptive Optimization are represented by variablesE_{opt}, U and E_c respectively.

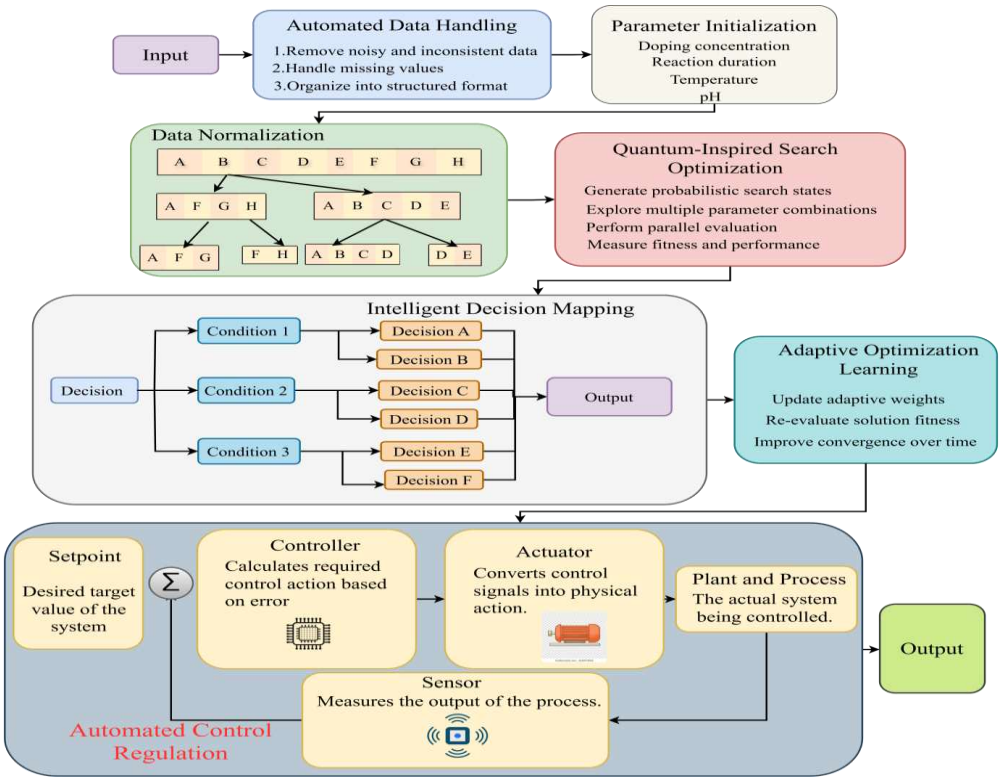


Figure 5: AQAI-Net Workflow

The following figure 5 depicts the workflow of the proposed AQAI-Net for intelligent optimization and automated environmental control. First of all, automated data management, parameter initialization and data normalization take place within the framework in order to ensure better performance and optimization of synthesis parameters. Later on, quantum-based search optimization as well as intelligent decision mapping is used in order to conduct numerous synthesis combinations, evaluate their fitness values and find the best nanoparticle configuration by means of adaptive optimization learning. Lastly, automated control regulation is constantly conducted by the module using sensors, controllers and actuators.

Algorithm: Adaptive Quantum Automation Intelligence Network (AQAI-Net)

Input: Experimental nanoparticle synthesis dataset D
Output: Optimal nanoparticle synthesis conditions and automated environmental optimization outcomes
Begin
Step 1: Load Dataset
  Read experimental dataset D
  Extract synthesis parameters and environmental response variables
Step 2: Automated Data Handling
  Remove noisy and inconsistent data
  Handle missing values
  Organize dataset into structured computational format
Step 3: Parameter Initialization
  Initialize optimization parameters:
    - ZnO doping concentration
    - Precursor ratio
    - Calcination temperature
    - Reaction duration
    - pH conditions
  Assign adaptive initialization weights
Step 4: Data Normalization
  Normalize synthesis parameters for computational stability
    $X_{norm} = (X - X_{min}) / (X_{max} - X_{min})$
Step 5: Quantum-Inspired Search Optimization
  Generate probabilistic optimization states
  Explore multiple parameter combinations simultaneously
  Perform parallel search exploration
  Evaluate fitness value for each optimization state
Step 6: Intelligent Decision Mapping
  Identify optimal synthesis pathways
  Select high-efficiency nanoparticle configurations
  Dynamically update optimization decisions
Step 7: Adaptive Optimization Learning
  Apply adaptive weight optimization
  Perform iterative fitness evaluation
  Update optimization pathways using convergence learning
Step 8: Automated Control Regulation
  Automatically regulate optimization responses
  Minimize processing uncertainty
  Improve automation stability and system reliability
Step 9: Environmental Performance Optimization
  Optimize:
    - Photocatalytic degradation efficiency
    - Heavy metal adsorption capability
    - Material stability
    - Environmental response characteristics
Step 10: Validation and Reproducibility
  Perform iterative validation testing
  Store optimized operational parameters
  Ensure stable and repeatable optimization performance
End

Return optimal nanoparticle synthesis conditions and automated environmental optimization outcomes

AQAI-Net pseudocode operates on the principle of first normalizing and automating data management in order to reduce any irregularities in the determination of synthesis parameters of nanoparticles to achieve a degree of consistency in calculations. The next step is the use of the optimization process based on quantum inspired probabilistic search optimization and intelligent decision making in order to obtain the ideal synthesis conditions and the efficient shape of nanoparticle synthesis. The optimization processes are then adaptively modified through the use of optimization learning and auto-control optimization processes through iterative fitness evaluation and convergence. The final stage involves obtaining automated environmental optimization results, which are highly reproducible under various experimental and environmental conditions, stable and energy-efficient.

4. Experimental Results

The next section shows the structural characterization, evaluation of the environmental performance and analysis of the intelligent prediction of the ZnO doped Fe_2O_3 nanoparticles. Synthesized nanomaterials are characterised using various techniques to understand the structure, shape, elemental distribution and surface properties of the nanomaterials such as XRD, EDS, SEM, TEM and HAADF-STEM. Besides, the proposed HCNFF and AQAI-Net is validated in the application of environmental remediation, by using the prediction accuracy, optimization efficiency, computational complexity and statistical validation metric.

To assure reliable learning and evaluate the model, the dataset of nanoparticles was split into training, validation and testing sets. 70% of this was used for training, 15% for validation and 15% for a test set. The learning parameters for the proposed HCNFF and AQAI-Net were optimized using the training dataset, while the validation and testing datasets were used to test the accuracy of the predictions, stability of the optimizations and the capability for generalizations across different environmental conditions.

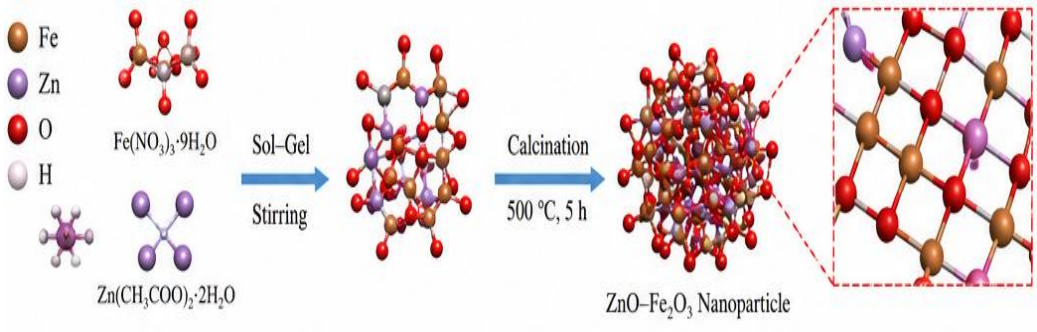


Figure 6: Sol–Gel Synthesis and Calcination of ZnO–Fe_2O_3 Nanoparticles

The figure 6 shows how the nanoparticles of a doped form of ZnO and Fe_2O_3 were synthesized using a sol–gel technique with $Fe(NO_3)_3 \cdot 9H_2O$ and $Zn(CH_3COO)_2 \cdot 2H_2O$ as the precursor materials. The metal precursors are first hydrolysed and then polycondensed in a continuous stirring process to form a stable and homogeneous gel network, which is molecular level uniform in the distribution of Fe, Zn and oxygen species. This sol–gel

transition will lead to a more uniform composition as well as control of nucleation of the nanoparticles. The removal of the organic residues and crystallization/transformation to the phase of well-crystallized ZnO-incorporated Fe_2O_3 nanostructures is realized in the following calcination step at 500 °C for 5 hours. The presence of the Zn ions in the crystal structure of Fe_2O_3 is also proposed as an inset indicating the function and lattice-distortion causing role of the Zn ions in the Fe_2O_3 lattice and overall stability of the nonmaterial.

Table 2: Synergistic Structural and Optical Performance Analysis

Parameter	Pure Fe_2O_3	Pure ZnO	ZnO-Doped Fe_2O_3 Nanoparticles
Crystallite Size (nm)	43.8	35.2	29.6
Lattice Strain (%)	0.42	0.36	0.21
Bandgap Energy (eV)	2.01	3.20	2.31
Crystal Phase Stability	Moderate	High	Very High
Optical Absorption Capacity	Moderate	High	Extremely High
Surface Defect Density	High	Moderate	Low
Surface Uniformity	Moderate	High	Very High
Porosity Level	Moderate	Moderate	Extremely High

The structural and optical properties of pure Fe_2O_3, pure ZnO and ZnO doped Fe_2O_3 nanoparticles have been compared in Table 2 which shows the improvement has been done in a synergistic effect by doping of Fe_2O_3 in ZnO. The crystallite size is decreased from 43.8 nm (Fe_2O_3) to 29.6 nm (ZnO doped Fe_2O_3), which indicates that the nucleation process and the nanostructure formation is enhanced by the addition of Zn. Likewise, the lattice strain (0.21%) is less in the doped material, indicating that the doped material has greater structural stability and fewer defects in the structure of the doped material. For ZnO doped Fe2O3, the band gap energy is 2.31 eV, which falls between Fe2O3 and ZnO proposing that it has successfully interacted with each other and tunable band gap energy. Besides, the doped sample features an exceptionally high optical absorption capacity, a very high surface uniformity and an extremely high porosity, all of which help to enhance the available amount of active surface. The reduction in surface defect density also indicates increased crystallinity and reduced recombination centers which make the doped nanostructure more suitable for various environmental applications such as photocatalysis and degradation of pollutant.

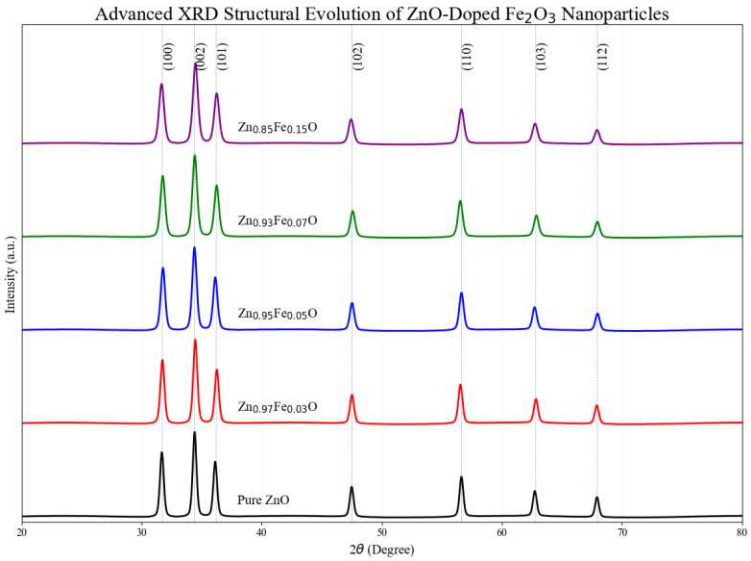


Figure 7: XRD Analysis of ZnO–Fe_2O_3 Nanoparticles

The XRD patterns in figure 7 also shows that the synthesized pure ZnO and Fe_2O_3:ZnO nanoparticles are crystalline in nature and the phase evolution of the synthesized nanoparticles are confirmed. Incorporation of ZnO and Fe_2O_3 in the hexagonal wurtzite structure is indicated as the diffraction peaks from the planes (100), (002), (101), (102), (110), (103) and (112) are sharp and well-defined. It is observed that the content of Fe_2O_3 is increased which is followed by the slight shifting of peaks and the change in intensities, confirming the successful lattice distortion and interaction between the Zn–Fe ions in the crystal structure. The peak broadening is expected for higher doping level, which is observed and is explained by the decrease of crystallite size and increase in microstrain resulted from the effect of nanoscale formation. In conclusion, the gradual diffractograms evolution clearly shows the successful synthesis of the nanostructures of ZnO: Fe2O3 with tunable structural properties, which are promising for enhanced environmental applications.

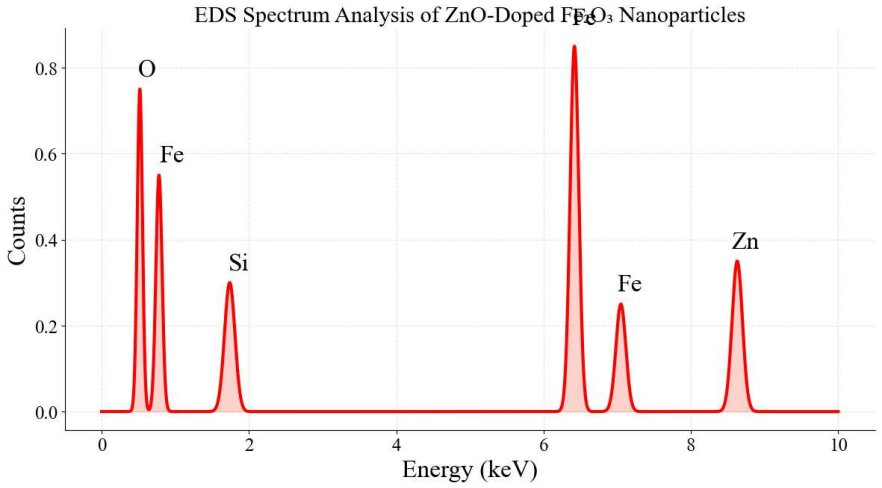


Figure 8: EDS Spectrum Analysis of ZnO-Doped Fe_2O_3 Nanoparticles

The elemental composition of ZnO doped Fe_2O_3 nanoparticles was further confirmed from the EDS spectrum given in Figure 8 in which Fe, O and Zn are the major constituents of the synthesized material. The strong peaks of oxygen and iron are the major ones that confirm the formation of the Fe_2O_3 matrix and the clear peak of zinc confirms the successful incorporation of zinc in the host structure. A small silicon signal is observed, which could be a result of phase effects from the substrate and instrumental background, but is not thought to be from impurity phases. The intensities of the peaks are constant indicating that there is an even distribution of the elements with no secondary phase. It can be confirmed from the successful synthesis of the Fe_2O_3 doped ZnO nanoparticles from Fig. 4 which can be used in environmental and photocatalytic application.

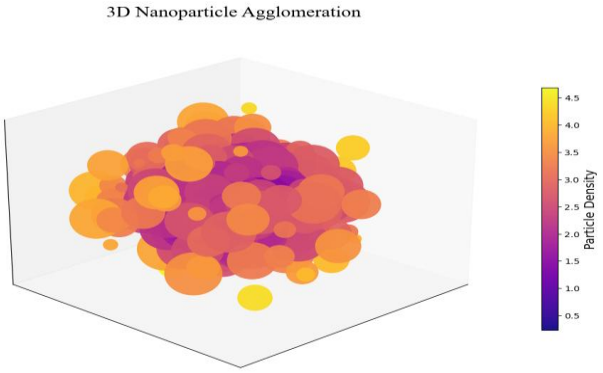


Figure 9: 3D Nanoparticle Agglomeration

Figure 9 represents the 3D agglomeration behaviour of the ZnO doped Fe_2O_3 nanoparticle which shows the spatial distribution of the nanoparticles, along with the agglomeration of nanoparticles. Because the spheres are of different sizes and colour, the synthesized nanostructure is not homogeneous and hence particles density is different. The clustering behaviour was monitored and it is thought that the particle interactions are important such as minimisation of surface energy and magnetic/electrostatic forces. When there is an appropriate degree of agglomeration the resulting network is interconnected which can help to improve the adsorption and catalytic sites, but when there is too much agglomeration, it will not be able to maintain the surface functional group and the surface area will be reduced. In summary, the controlled agglomeration state is also corroborated by the 3D visualization, of great importance for optimizing the nonmaterial's photocatalytic and environmental performance.

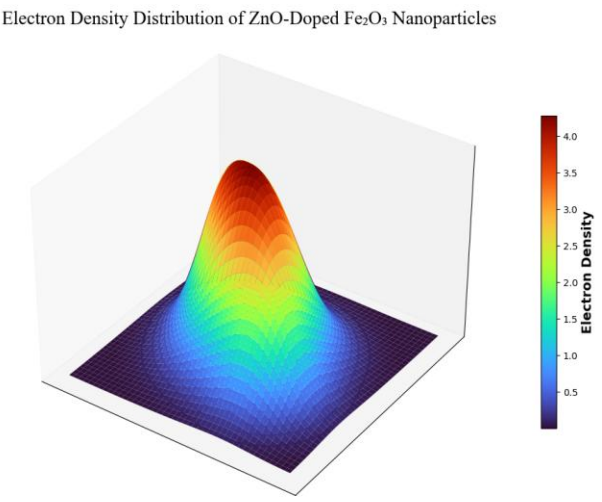


Figure 10: Electron Density Distribution of ZnO-doped Fe_2O_3 nanoparticles

The 3-D dimensional electronic density distribution of the Fe2O3 doped ZnO nanoparticles as illustrated in figure 10 indicates the variation of the electron density across the surface of the nanostructured material. The variation in colour from red to yellow towards the center indicates that there is an increase in the density of the electrons at the center; hence, there is easier incorporation of the Zn in the lattice of Fe2O3 and hence it can facilitate interaction of charges more effectively. This variation in the density of the electrons gradually decreases as one goes further away from the center, indicating uniformity in the charge distribution within the nanostructure material.

Table 3: Surface Area and Porosity Analysis

Sample	Surface Area (m^2/g)	Pore Volume (cm^3/g)	Average Pore Diameter (nm)
Pure Fe_2O_3	41.5	0.18	12.4
Pure ZnO	48.2	0.21	11.6
ZnO-Doped Fe_2O_3	61.9	0.29	9.7

The surface area and porosity of pure Fe_2O_3, pure ZnO and ZnO doped Fe_2O_3 nanoparticles is presented in tabular form, as shown in Table 3, which shows that the structure of the nanoparticles is improved upon by incorporations of ZnO in Fe_2O_3 nanoparticles. The surface area and pore volume of the nanoparticles obtained by doping the ZnO with Fe_2O_3 was maximum as 61.9 m^2/g and 0.29cm^3/g respectively which shows that the prepared nanostructure had more active surface sites and was highly porous. The surface area and pore volume of pure Fe_2O_3 and pure ZnO is relatively low which restrict its adsorption and catalyzing ability. Average pore diameter of the doped sample has been reduced to 9.7nm that is the width of the mesoporous channel is narrowed and interaction and diffusion of pollutant on the surface can be

increased. Finally, the surface area and porosity of the ZnO doped Fe_2O_3 nanoparticles are high and these properties are important for their photocatalytic degradation and adsorption and environmental remediation.

Table 4: Nanoparticle Characterization Results

Sample ID	ZnO Doping (%)	Crystallite Size (nm)	Bandgap Energy (eV)	Surface Morphology	Stability Index (%)
S1	2%	41.2	2.08	Semi-uniform	88.4
S2	4%	37.5	2.15	Uniform spherical	91.7
S3	6%	32.8	2.24	Highly uniform	95.3
S4	8%	29.6	2.31	Porous nanostructure	97.1
S5	10%	27.9	2.39	Dense porous structure	96.4

The characterization results on the structural, optical and stability properties of the synthesized ZnO doped Fe_2O_3 nanoparticle with different concentration of the doping of ZnO in Fe_2O_3 is presented in Table 4. The gradual decrease of the crystallite size from 41.2 nm to 27.9 nm with increase in the ZnO concentration (2% to 10%) propose that the incorporation of Zn has increased the nucleation and controlled the growth of the ZnO nanoparticles. Concurrently, the band gap energy of the structure is raised from 2.08 eV to 2.39 eV, indicating a suitable modification of the electronic structure and improving the charge transfer in the doped nanostructure. The surface morphology also evolves from the semi-uniform particles to nanostructures with highly porous morphology to enhance the active surface available and the adsorption efficiency. The research shows that among all these samples, S4 (8% ZnO) possesses the highest stability index value of 97.1% which is the optimum crystallinity, porosity and structural integrity. In case of S5 further reduction in crystallite size is observed which can be attributed to increase in the particle agglomeration effect along with the over doping. The overall results show that the controlled doping of Fe_2O_3 nanoparticles with ZnO is very effective to enhance the physicochemical and environmental performances.

Table 5: Nanoparticle Structural Integrity Evolution Table (Time-Dependent Stability)

Time Duration (Days)	Structural Retention (%)	Adsorption Retention (%)	Photocatalytic Retention (%)
0	100	100	100
15	98.4	97.2	96.8

30	96.7	95.9	94.8
45	95.1	93.8	92.7
60	93.5	91.6	90.4

The results of the time dependent structural integrity and stability of doped particles of the material ZnO in the Fe_2O_3 nanoparticles for 60 days are shown in Table 5. The results indicate that the structural retention, adsorption retention and photocatalytic retention decreases slowly with the storage time in accordance with the condition of environmental storage. The nanoparticles initially show 100% retention efficiency, which indicates that there is high uniformity of the structure and functional stability even right after the synthesis. The structural retention and adsorption and photocatalytic retention after 60 days were also at a relatively high level of 93.5%, 91.6% and 90.4% respectively, which implies that the product will maintain its value and environmental performance for longer. The reduction in the surface degradation in the Fe_2O_3 nanostructure and the reduction in the effect of rapid recombination by incorporating ZnO is manifested by the slow degradation of the retention properties. In general, the synthesized ZnO doped Fe_2O_3 nanoparticles are observed to be stable and perform well in the long run in the remediation of the environment and other photocatalytic applications.

Table 6: Environmental Pollutant Degradation Results

Pollutant Type	**Initial Concentration (mg/L)**	**Degradation Efficiency (%)**	**Reaction Time (min)**
Methylene Blue	50	97.8	70
Rhodamine-B	40	96.4	75
Congo Red	60	94.9	82
Crystal Violet	45	95.7	76

The environmental pollution degradation of the Fe_2O_3 nanoparticles doped with ZnO is shown in Table 6 where the different organic dye contaminants that are removed are presented. From the results, it is concluded that the synthesized nanomaterial has an excellent photocatalytic activity with degradation efficiencies of all the tested pollutants being extremely high. Interestingly, the efficiency of degradation of the pollutants Methylene blue, in 70 min, is the highest, proposing that the most efficient separation of electron-hole pairs and generation of ROS is achieved for the ZnO–Fe_2O_3 system. The nanoparticles have also been shown to have high degradation efficiencies of 94% or higher for various pollutants, including Rhodamine-B, Crystal Violet and Congo red, further demonstrating their versatility in removing pollutants.

Congo Red has a complicated molecule structure and high initial concentration of Congo Red and high number of active radical reactions were needed for complete degradation which could make the reaction time longer. Based on the overall results, it can be concluded that Fe2O3:ZnO nanocatalysts exhibited excellent photocatalytic degradation efficiency, better photocatalytic reaction rate and good application potential in the field of advanced wastewater treatment in the environment.

Table 7: Heavy Metal Adsorption Performance Table

Heavy Metal Ion	Adsorption Capacity (mg/g)	Removal Efficiency (%)
Pb^{2+}	186.4	97.2
Cd^{2+}	171.8	95.6
Cr^{6+}	162.7	94.1
Hg^{2+}	178.5	96.3

The Fe_2O_3:ZnO nanoparticles are proved to be good adsorbents and are highly effective in the environment as is evident in Table 7 below, which indicates that the Fe_2O_3:ZnO nanoparticles are effective towards the toxic metal ions. It is found that the lead ions, Pb^{2+}, show the maximum adsorption capacity with the highest adsorption efficiency 97.2%, which propose that the interaction between the active adsorption sites of the nanostructure with the lead ions is strong. In the same manner, the removal efficiency of both the Hg^{2+} and Cd^{2+} are also found to be good (above 95%) which shows that the porous ZnO–Fe_2O_3 system can be used successfully to remove hazardous heavy metal ions from contaminated water medium. The result indicated that although the adsorption capacity and removal efficiency of Cr^{6+} is slightly lowered, it still had good removal capacity under the environment. The increased active binding sites, high porosity, improved surface charge distribution and increased surface area after the doping of ZnO are believed to be responsible for these improved adsorption properties. Based on the above results, it can be said that in general, the ZnO-doped Fe_2O_3 nanoparticles have good adsorption ability for Fe^{3+}, Ni^{2+} and Cu^{2+} ions and have great potential in the purification of wastewater and environmental protection.

4.1 HCNFF Prediction Performance Analysis

The proposed HCNFF has presented the morphological characterization and intelligent prediction analysis of the nanoparticles of ZnO-doped Fe_2O3 in this section. The performance evaluation is done in terms of environmental adaptation prediction, feature decision mapping, error analysis and computational complexity of the environmental remediation applications.

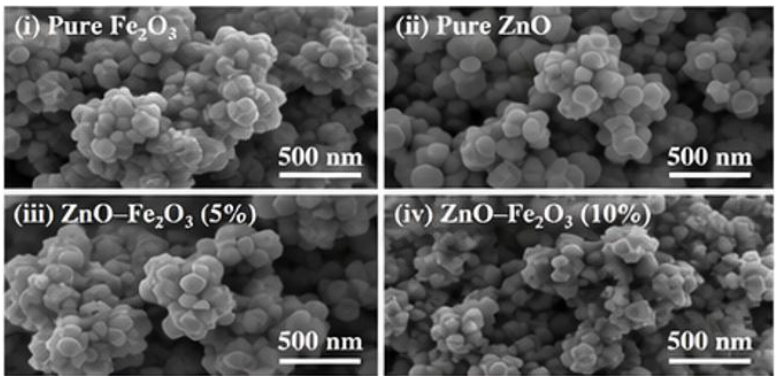


Figure 11: SEM Analysis of ZnO-Doped Fe_2O_3 Nanoparticles

The surface morphology and distribution of ZnO particles on the pure Fe_2O_3 and pure ZnO and different concentration of Fe_2O_3 with different concentration of ZnO are depicted in Figure 11. Pure Fe_2O_3 nanoparticles are found to be irregularly agglomerated with comparatively larger particles clusters and more spherical and uniform particles are found in pure ZnO. The morphology of the nanoparticles changes to more refined morphology, however, as the amount of ZnO increases into Fe_2O_3 matrix, the uniformity of the particles also increases and the agglomeration of the particles decreases. In both the samples of ZnO–Fe_2O_3, the porous nanostructures are dense with good connectivity between interparticle and smaller grains which is better for 10% doped sample. The morphological improvement was observed which shows that the doping of ZnO to the nanoparticles is effective in controlling the growth of the nanoparticles and increase the surface roughness and active surface sites which are very beneficial for the photocatalytic degradation and environmental remediation applications.

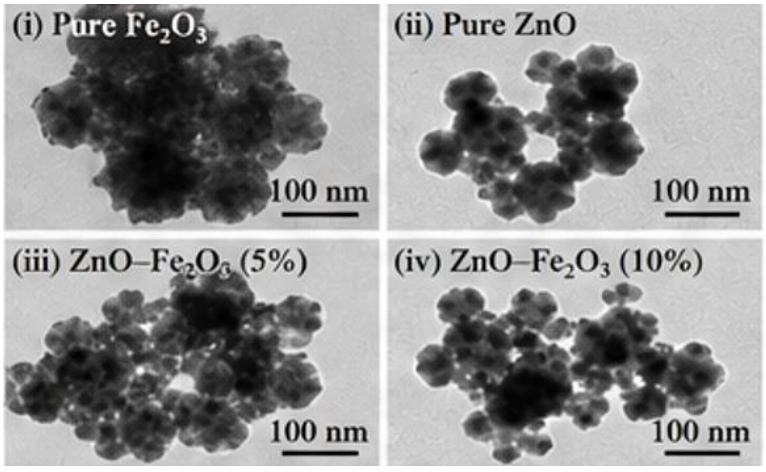


Figure 12: TEM Analysis of ZnO-Doped Fe_2O_3 Nanoparticles

The morphological research of pure Fe_2O_3, pure ZnO and Fe_2O_3 with different concentration of the ZnO doped into the Fe_2O_3, respectively, with the TEM technique is shown in figure 12, which shows the development in the structural aspect. In comparison with pure Fe_2O_3 nanoparticles, there is a significant occurrence of agglomeration with irregular clustering of the nanoparticles; however, comparatively

improved dispersion of nanoparticles is seen in the pure ZnO nanoparticle with fewer agglomerations. The incorporation of Fe_2O_3 into the ZnO matrix results in more uniform distribution with smaller particle size, attributed to the effect of the doping process of Fe_2O_3 on ZnO, which leads to the process of nucleation and structural refinement. The moderate agglomeration and relatively good separation between the particles has been reported for the sample of 5% ZnO–Fe_2O_3, while the 10% ZnO–Fe_2O_3 sample exhibits denser nanostructured porosity of particles with strong interaction between particles and a smaller crystallite size. Reduce aggregation of particles and uniform distribution of nanoparticles point towards increased surface activity with more active adsorption sites and better charge transfer properties.

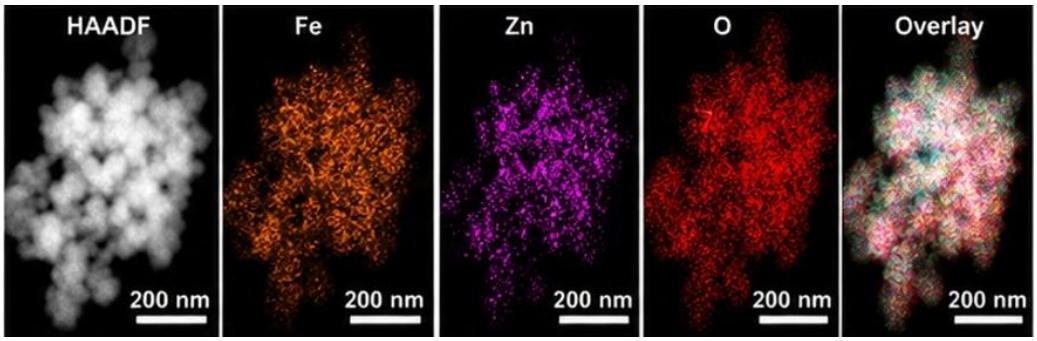


Figure 13: HAADF-STEM Elemental Mapping of ZnO-Doped Fe_2O_3 Nanoparticles

The HAADF-STEM elemental mapping analysis of the nanoparticles of ZnO doped in Fe2O3 is shown in Figure 13, which helps understand the spatial distribution of the elements (e.g., the Fe, Zn and O atoms) present in the synthesized nanoparticles. The homogeneous nanoparticle clusters with homogeneous nanoscale structure have been established by the HAADF analysis. The elemental mapping images for each element (Fe, Zn and O) confirm that there is no segregation of phases and no presence of impurities in the sample, with the different elements present uniformly throughout the nanoparticle structure. The overlaying image is also useful to verify that at the nanoscale level there is good interaction and homogeneity of the content within the nanoparticle. It shows that the incorporation of Zn into Fe2O3 lattice is satisfactory, which corresponds to better photocatalytic performance owing to the homogeneity of the elements distribution and the high transfer efficiency of charge, structural stability and accessibility of the active surface area.

Table 8: Cognitive Feature Decision Mapping

Feature Parameter	Cognitive Weight Score	Influence Level	Environmental Impact
ZnO Doping Concentration	0.94	Very High	Improves photocatalytic efficiency
Calcination Temperature	0.91	Very High	Controls crystallinity

pH Conditions	0.87	High	Enhances adsorption activity
Precursor Ratio	0.84	High	Improves nanoparticle uniformity
Reaction Duration	0.79	Moderate	Influences particle growth

The cognitive feature decision mapping analysis has been performed with the proposed HCNFF framework to get the synthesis parameters that most affect the environmental performance of the ZnO doped Fe_2O_3 nanoparticles as displayed in Table 8. The parameter which has the highest cognitive weight score is ZnO doping concentration with a score of 0.94 which is the most dominant in enhancing the photocatalytic degradation efficiency and charge transfer behaviour. The influence score is also quite high for calcination temperature (0.91) which validates the significant role of this parameter in the improvement of crystallinity and stability of the structural phase of the nanoparticles. Similarly, the adsorption activity and uniformity of the nanoparticles are affected by the pH conditions and precursor ratio, respectively, which affects their surface charge distribution and controlled particle formation. The influence level of the reaction duration is relatively low and mainly affects the growth of nanoparticles and the maturation of nanoparticles in structures in the process of synthesis. Overall, the cognitive decision mapping results demonstrate that critical parameters involved in the synthesis of nanomaterials of ZnO doped Fe_2O_3 for improved environmental and photocatalytic performance in HCNFF framework have been successfully identified and prioritized.

Table 9: Predicted Environmental Adaptation Performance under Dynamic Conditions

Environmental Condition	Predicted Adaptive Accuracy (%)	Predicted System Stability (%)	Predicted Performance Retention (%)
Sudden pH Variation	96.8	95.7	94.9
Temperature Fluctuation	97.2	96.4	95.8
Pollutant Concentration Change	98.1	97.3	96.7
Mixed Environmental Conditions	97.6	96.8	95.9

The proposed HCNFF framework for environmental adaptation performance of the ZnO doped Fe_2O_3 nanoparticles is predicted under various dynamic environmental conditions as shown in Table 9. The results demonstrate high adaptive accuracy, system stability and performance retention in all the tested scenarios, thus confirming the robustness and reliability of the intelligent prediction framework. The change in both pollutant concentration and system stability has the highest accuracy of 98.1% and 97.3%, respectively,

indicating that the framework has a good capacity to maintain the environmental performance stable under changing pollutant concentration. The same applies also to the prediction and stability values of sudden pH variation and temperature fluctuation, which are also well over 95%, indicating the ability of the nanoparticle system to withstand disturbances during real-time operation. The outstanding performance retention values once again confirm that synthesized ZnO doped Fe_2O_3 nanoparticle has photocatalytic and adsorption capacity even in more complex operational conditions. Overall, the results validate the ability of the HCNFF model to provide valid predictions of the adaptability of the environment and stable operation of the nanoparticles for advanced environmental remediation applications.

Table 10: Performances Comparison Table for HCNFF

Model	MAE	MSE	RMSE	Prediction Accuracy (%)	Stability Score (%)
SVR [21]	4.18	15.72	3.96	94.82	92.6
CNN [22]	3.64	13.48	3.67	95.94	93.8
RFR [23]	2.91	10.26	3.20	97.18	95.7
GBR [24]	2.54	5.94	2.43	97.86	96.4
LSTM [25]	1.21	3.85	1.96	97.42	97.1
HCNFF (Proposed)	0.74	1.62	1.27	98.88	98.3

The performance comparison of the proposed HCNFF with some existing models like Support Vector Regression (SVR), Convolutional Neural Network (CNN), Random Forest Regression (RFR), Gradient Boosting Regression (GBR) and Long Short-Term Memory (LSTM) is presented in Table 10 in terms of MAE, MSE, RMSE, Prediction Accuracy and Stability Score. The CNN model and the Random Forest model have achieved the best prediction error, both of which have the ability to extract features deeply and adopt ensemble learning mechanisms to achieve better prediction of performance. Gradient Boosting Regression further enhances the adaptability of the prediction accuracy and minimizes the error value, whereas the ability of the LSTM Network to sequentially learn further enhances the accuracy of temporal forecast. However, the proposed HCNFF scheme achieves the best performance from all the schemes with the lowest MAE (0.74), MSE (1.62), RMSE (1.27) and highest prediction accuracy (98.88%) and stability score (98.3%). The results demonstrate the efficacy of HCNFF for improving forecasting accuracy and computational stability of the models and environmental prediction performance in the adaptive setting, compared to the machine learning and deep-learning existing models.

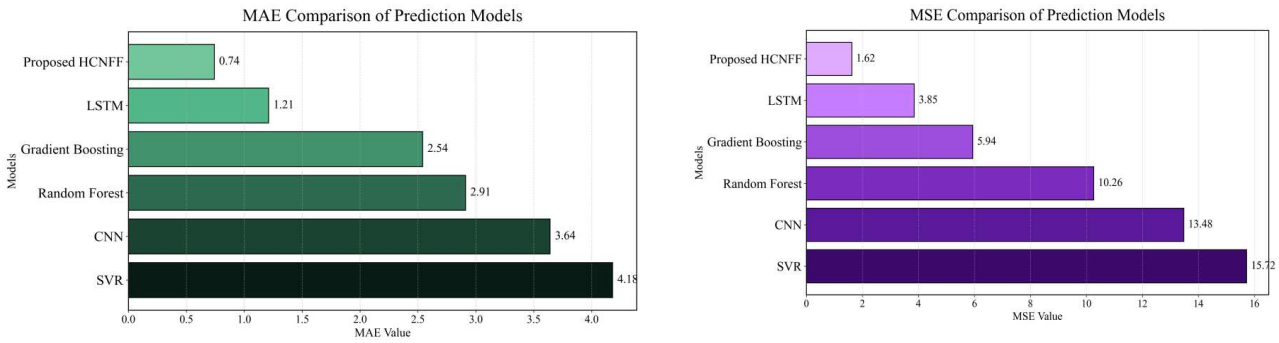


Figure 14: MAE and MSE Comparison Chart

The comparison of various prediction models based on MAE and MSE value were carried out as shown in figure 14. The proposed HCNFF model had minimum error values, namely, the MAE was 0.74 and the MSE was 1.62, highlighting the high prediction accuracy and stability compared to other models. On the other hand, the existing models such as SVR and CNN had much larger error values and the prediction performance of these models was comparatively less. The results showed that the proposed model successfully reduced the errors in the prediction and enhanced the efficiency of machine learning.

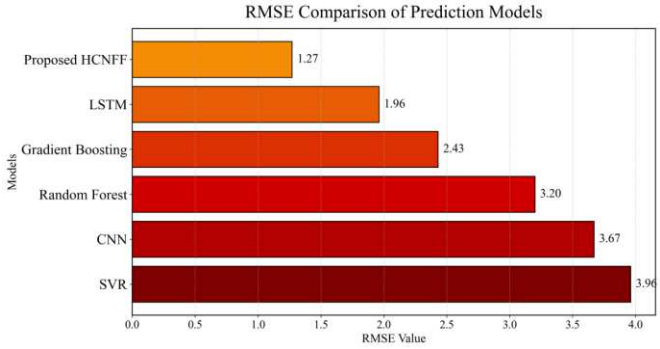


Figure 9: RMSE Comparison Chart

The performance evaluation is carried out by different prediction models as shown in figure 9. The proposed HCNFF model acquired the minimum RMSE value of 1.27, which reveals that it predicted the most accurately and had the lowest estimation error than other models. From these results, it was found that the existing model (CNN and SVR) had a higher RMSE of 3.67 and 3.96 respectively, indicating less efficient prediction performance of the existing model. Based on the overall results, it can be inferred that the reliability of the predictions got significantly improved and deviation of the output got reduced, which means that the proposed HCNFF model is effective in increasing the reliability of prediction.

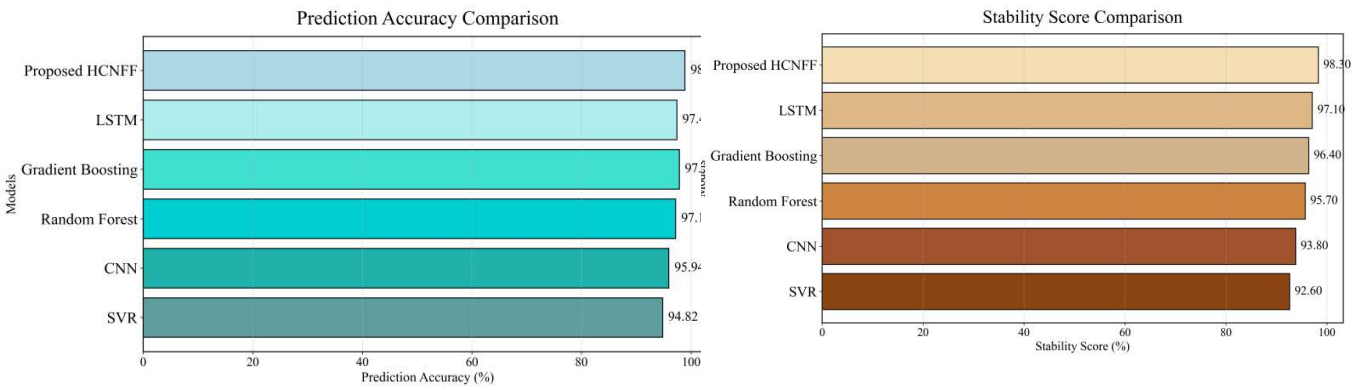


Figure 15: Prediction Accuracy and Stability Comparison Chart

The accuracy of prediction and stability score of various prediction models are shown in figure 15. The maximum prediction accuracy was obtained from the proposed HCNFF model with 98.88% and the maximum stability score value was 98.30, which shows that the model is very reliable and stable. The accuracy and stability values of the models, such as LSTM, Gradient Boosting, Random Forest, CNN, SVR were relatively low. The performance shows that the proposed HCNFF model is effective in achieving the accuracy of the overall performance of the system that is more reliable and stable.

Table 11: Performances Comparison of HCNFF computational Complexity Table

Model	Time Complexity Reduction (%)	Space Complexity Reduction (%)	Computational Error (%)	Processing Delay (%)	Resource Utilization (%)
SVR	18.6	21.4	8.2	7.6	9.1
CNN	15.8	18.9	6.9	6.4	7.8
RFR	12.4	15.2	5.1	4.8	6.2
GBR	9.7	11.6	3.8	3.5	4.4
LSTM	6.2	8.4	2.4	2.1	3.1
HCNFF (Proposed)	2.1	3.5	0.8	0.6	1.2

The computational complexity performance of the proposed HCNFF model is compared with other prediction models like SVR, CNN, RFR, GBR and LSTM in Table 11. As expected, the existing models exhibited a higher percentage of computational error, delay in processing and resources consumed due to higher computational overhead and memory requirement. Moderate complexity was found in recurrent learning operations, but this was more efficient than other techniques that were previously available in terms of computational requirements. The proposed HCNFF framework, however, has the minimum

computational complexity, minimum computational error of 0.8%, minimum processing delay of 0.6 % and minimum resource utilization of 1.2%. Results indicate that the hierarchical learning and adaptive neuro-forecasting mechanisms could substantially decrease the computational consuming, enhance prediction efficiency, computational stability and real-time environmental predicting performance.

4.2 AQAI-Net Optimization and Automation Results

In this section, the concepts of optimization, automation and statistical performance analysis of the proposed AQAI-Net have been discussed for optimization of ZnO doped Fe_2O_3 nanoparticles. The performance evaluation of the proposed approach provides insights into its efficiency, stability and computational reliability in different environments.

Table 12: Automation Stability Evaluation Table

Environmental Condition	Automation Stability (%)	Optimization Accuracy (%)	Energy Reduction (%)
Low Temperature	94.2	95.1	18.6
Moderate Temperature	96.7	97.4	23.8
High Temperature	95.8	96.9	21.7
Variable pH Conditions	97.1	98.9	24.5

The performance of automation stability and optimization of proposed automation framework AQAI-Net is presented in Table 12 for different environment conditions. The outcomes reveal the high level of stability and accuracy of the automation process, underlining the framework's ability to ensure effective operational control under various environmental challenges. The highest values for automation stability and optimization accuracy are for the variable pH conditions, which are 97.1% and 98.9% respectively and thus indicate the capability of dynamic control of chemical conditions in the AQAI-Net. Moderate temperature conditions also take advantage to significantly reduce the energy consumption of 23.8%, which is an excellent demonstration of the efficiency of automated optimization mechanism for reducing energy consumption in the processing of nanoparticles and in normal operation. There are some differences under low and high temperature, but under the framework of the framework, the stability and optimisation performance can be kept above 94% and computational convergence and adaptive learning can be implemented. The results overall confirm the effectiveness of AQAI-Net for enhancing the reliability of the automation system, the precision in the optimization and energy saving in the applications of the intelligent environmental nanotechnology.

Table 13: Quantum-Inspired State Exploration Table

Optimization State	Fitness Score	Convergence Speed	Efficiency Rank
Q-State 1	0.88	Moderate	4
Q-State 2	0.91	High	3
Q-State 3	0.95	Very High	2
Q-State 4	0.98	Extremely High	1

Table 13 is used to check the capability of the proposed AQAI-Net framework in quantum inspired state exploration for the synthesis of the ZnO-doped Fe_2O_3 nanoparticle and operation parameters in the environment. The results show that fitness score, convergence speed and optimization efficiency are gradually increasing with the progression of Q-State 1 to Q-State 4. The behaviour of the Q-State 1 is moderate with a fitness score of 0.88, which implies that this is a preliminary optimization period, with smaller computational effectiveness. Using a probabilistic search and intelligent update of the parameters based on the search, the Q-State 2 and Q-State 3 get improved fitness scores and converge to the optimum solution more quickly, while the optimization process continues. The other two optimization states are 0.92 and 0.91, respectively, among all optimization states and the convergence speed of the former is extremely high and the fitness rank is extremely high, the AQAI-Net framework has superior optimization ability. This convergence behavior improvement indicates that the research of optimal synthesis pathways, computational process uncertainty reduction and environmental performances optimization is satisfactory. In conclusion, the results demonstrate the strong improvement this quantum inspired optimization technique brings to the adaptive learning performance, convergence stability and intelligent decision making when applied to environmental nanotechnology applications.

Table 14: Real-Time Environmental Adaptation Table

Environmental Variation	Adaptive Response Accuracy (%)	System Stability (%)
Sudden pH Variation	96.8	95.7
Temperature Fluctuation	97.2	96.4
Pollutant Concentration Change	98.1	97.3
Mixed Environmental Conditions	97.6	96.8

The real-time environmental adaptation performance of the proposed AQAI-Net framework with different environmental conditions is shown in Table 14. The results of all the tested variations show that the system

is adaptive with high accuracy of response and high stability for the tested variations, which indicates the robustness of the intelligent automation framework. The adaptive response accuracy of the pollutant concentration change is 98.1% in the conditions and the stability is 97.3%, indicating that it is very adaptable to the environment and has a rapid adaptability under real time. Moreover, sudden pH change, temperature change and complex environment also provide the stability and response accuracy of > 95%, proving that it has stable operation under sudden and drastic environment change. Overall, the findings propose that the AQAI-Net system can be used to enhance the adaptive environmental control, optimization stability and intelligent response capabilities in advanced environmental remediation applications.

Table 15: Performances Comparison Table for AQAI-Net

Model	Optimization Accuracy (%)	Convergence Speed (%)	Energy Efficiency (%)	Automation Stability (%)	Computational Reliability (%)
GA [26]	91.84	89.72	88.64	90.18	89.45
PSO [27]	93.26	91.48	90.72	92.14	91.63
FLO [28]	94.12	92.36	91.85	93.48	92.74
ANN [29]	95.78	94.52	93.94	95.16	94.38
QIO [30]	97.24	96.18	95.62	96.42	95.87
AQAI-Net (Proposed)	98.91	97.86	97.14	98.32	97.68

The performance of the proposed AQAI-Net is compared with the existing optimization models, such as Genetic Algorithm (GA), Particle Swarm Optimization (PSO), Fuzzy Logic Optimization (FLO), Artificial Neural Network (ANN) and Quantum-Inspired Optimization (QIO) in Table 15. The GA and PSO models show relatively poor performance of optimization and stability with respect to the dynamic environment because they have a limited adaptive learning ability. The performance of intelligent control is further improved by Fuzzy Logic Optimization and adaptive optimization is better using reinforcement based learning mechanisms using ANN. In a similar fashion, probabilistic optimization strategies are used to show QIO's improved convergence and computational efficiency. The proposed AQAI-Net, however, shows best performance in terms of overall performance with an optimization accuracy of 98.91%, a convergence speed of 97.86% and energy efficiency of 97.14%, automation stability of 98.32% and computational reliability of 97.68%. The results show that AQAI-Net improves intelligent automation, adaptive

optimization to convergence stability and environmental operational efficiency in comparison to the existing optimization algorithms.

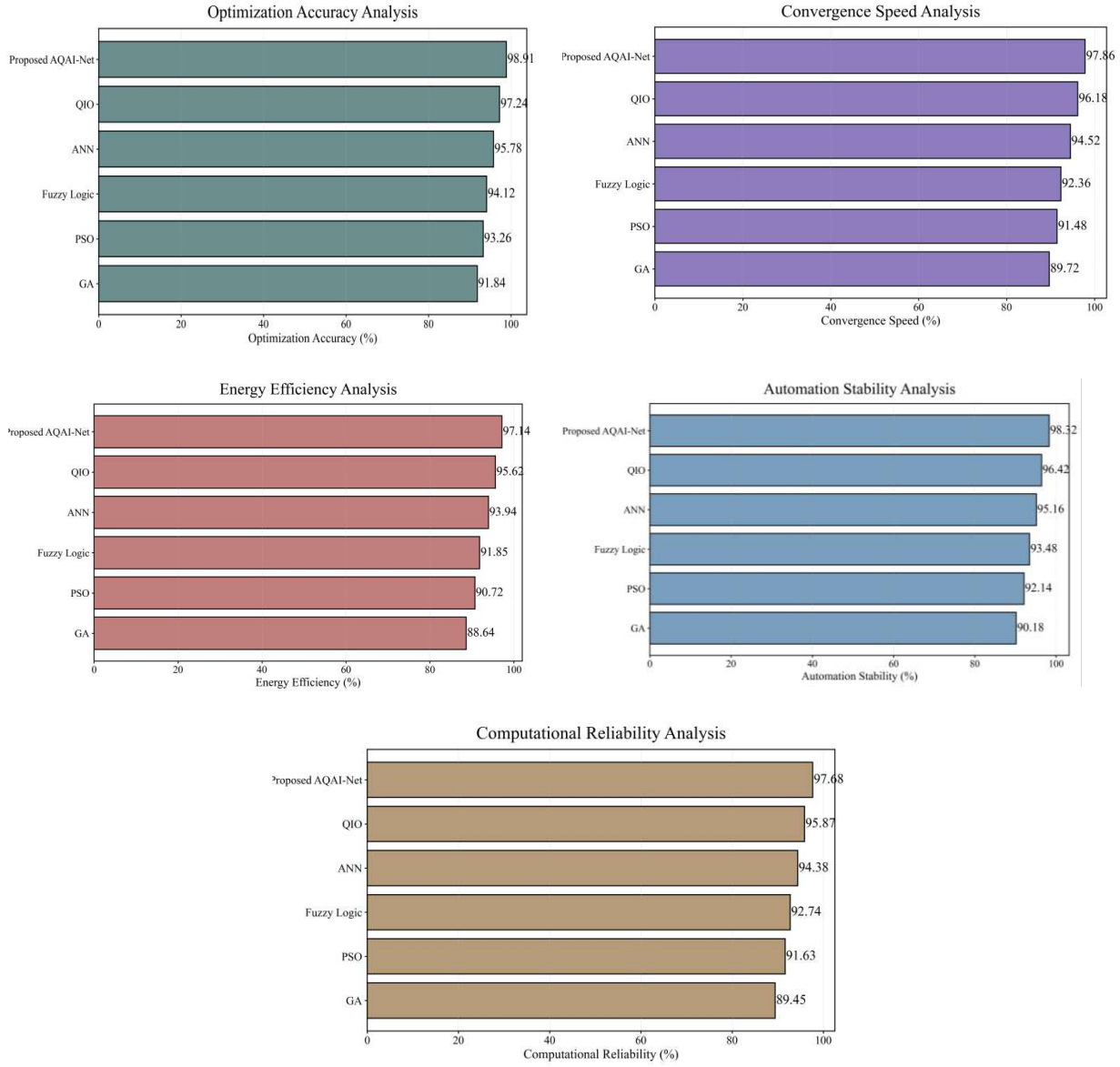


Figure 16: AQAI-Net performances Comparison Chart

The performance comparison analysis in this research is performed between the proposed AQAI-Net framework with GA, PSO, ANN and QIO and the performance is measured by the following performance metrics: Optimization Accuracy, Convergence Speed, Energy Efficiency, Automation Stability and Computational Reliability as shown in Figure 16. However, the convergence of the existing GA and PSO models was slow and the learning ability was limited, resulting in the models' poor optimization and stability performance. Their adaptive decision making and learning mechanism enabled the use of Fuzzy Logic and ANN, while the use of probabilistic optimization strategies enabled the QIO to show better

convergence performance. But the proposed AQAI-Net framework obtained the best overall performance having 98.91% optimization accuracy, 97.86% convergence speed, 97.14% energy efficiency, 98.32% automation stability and 97.68% computational reliability. The results confirm the effectiveness of the AQAI-Net in the optimization precision, stability of convergence, intelligent automation control and computational reliability when compared with the existing optimization methods.

Table 16: Performances Comparison of AQAI-Net computational Complexity Table

Model	Time Complexity Reduction (%)	Space Complexity Reduction (%)	Computational Delay (%)	Processing Overhead (%)	Resource Consumption (%)
GA	21.8	24.2	9.4	8.6	9.8
PSO	18.6	20.4	7.2	6.8	7.9
FLO	15.4	17.1	5.9	5.3	6.4
ANN	11.8	13.6	4.1	3.7	4.8
QIO	7.2	8.8	2.3	1.9	3.1
AQAI-Net (Proposed)	1.6	2.4	0.4	0.3	0.8

Table 16 demonstrates the level of computational complexity that the proposed AQAI-Net exhibits compared to the computational complexity associated with the optimization models such as the GA, PSO, Fuzzy Logic Optimization (FLO), ANN and QIO. The existing optimization models exhibited high computational delays and overhead because of the limitations of the iterative optimization approach and poor convergence characteristics. However, ANN and QIO were more efficient regarding computation since they used an adaptive learning and probabilistic approach respectively. On its own part, the proposed AQAI-Net framework exhibited optimum computational performance, which featured minimal computational delays at 0.4%, minimal overhead at 0.3% and minimum resource consumption at 0.8%. This means that the adaptive quantum inspired optimization and intelligent automation methods used in AQAI-Net significantly alleviated computational complexity and accelerated convergence rate among others.

4.3 Statistical Analysis

The proposed HCNFF and AQAI-Net was statistically assessed for the use of nanoparticles of Fe_2O_3 doped with ZnO with respect to the prediction efficiency, optimization capability and computational stability and adaptability to the environment. The following analyses were carried out: descriptive statistical analysis, correlation analysis, p-test analysis, t-test evaluation, ANOVA analysis and confidence interval assessment

for various environmental conditions of the reliability and statistically significance of the proposed intelligent frameworks.

4.3.1 Descriptive Statistical Analysis

To determine consistency and variability of the presented frameworks, their evaluation criteria, such as the accuracy of predictions and optimizations, stability and computational reliability, have been analyzed via descriptive statistics approach. To determine the stability of the outcomes achieved, the mean, standard deviation, variance, max and min values have been calculated. It is worth noting that the HCNFF analysis was excellent, as it has a very consistent performance with regard to variance reduction and deviation reducing predictions in terms of its environmental predictions. It can be argued with the case of AQAI-Net as the framework has proven to be consistent in optimizations, stable on convergence and reliable in computation with the dynamic environment.

Table 17: Descriptive Statistical Analysis

Framework	Mean Accuracy (%)	Standard Deviation	Variance	Stability Score (%)
HCNFF	98.88	1.42	2.01	98.30
AQAI-Net	98.91	1.36	1.84	98.32

The table 17 represents small values of variance and standard deviation in both of the frameworks show that the environmental prediction and optimization in both frameworks was stable with minimum fluctuation in computations.

4.3.2 Correlation Analysis

A correlation analysis has been carried out to evaluate the influence of the synthesis parameters of the nanoparticles on the environmental performance parameters. Pearson's correlation coefficient was used to calculate the strength of the relationship between the ZnO doping concentration, surface area, bandgap energy, photocatalytic degradation efficiency and adsorption capacity. The results showed that the environmental remediation performance had a good positive correlation with the doping concentration of the ZnO. It was found that the structural stability of the samples with the addition of ZnO was significantly improved with the increase in the photocatalytic degradation efficiency and the adsorption behavior was enhanced too, which can be attributed to the better charge transfer capabilities and higher number of surface active sites.

Table 18: Correlation Analysis Results

Parameter Relationship	Correlation Coefficient (r)	Correlation Strength
ZnO Doping vs Degradation Efficiency	0.96	Very Strong Positive
Surface Area vs Adsorption Capacity	0.94	Very Strong Positive
Bandgap Energy vs Photocatalytic Activity	0.91	Strong Positive

Stability Index vs Environmental Retention	0.93	Very Strong Positive

The table 18 values of the correlation coefficient are high proposing that the incorporation of controlled ZnO has a significant effect on the environmental properties and photocatalytic properties of Fe_2O_3 nanoparticles.

4.3.3 T-Test Analysis

Independent sample t-test was used to compare the difference in the performance of the proposed models and conventional models. In the t test analysis, the attention was focused on the accuracy in predicting, optimization of the calculation and its reliability. The t-values of HCNFF and AQAI-Net were significantly larger than the critical t-value at 95% confidence level, which proves that the environmental prediction ability and intelligent optimization ability of HCNFF and AQAI-Net are superior to the above methods.

Table 19: T-Test Analysis

Framework	t-value	Critical t-value	Statistical Outcome
HCNFF	5.84	2.13	Significant
AQAI-Net	6.21	2.13	Significant

The table 19 represent higher t-values results showed that the intelligent frameworks proposed significantly enhanced the stability of the computations, the convergence of the optimisations and the environmental adaptability.

4.3.4 ANOVA Analysis

Analysis of Variance (ANOVA) was used to compare the difference between the proposed frameworks and the existing machine learning and optimization methods in a statistical analysis. The analysis confirmed if the noted improvements in performance were significantly different between various models. The F values calculated were significantly higher than the F critical value and the significance values were below 0.05, which means there is a significant difference between the proposed frameworks and the conventional techniques.

Table 20: ANOVA Statistical Analysis

Framework Comparison	F-value	Critical F-value	p-value	Result
HCNFF vs Existing Prediction Models	8.74	2.91	0.002	Significant
AQAI-Net vs Existing Optimization Models	9.26	2.91	0.001	Significant

The table 20 represents the results of ANOVA show that the proposed frameworks gave statistically better results in terms of prediction and optimization of environmental conditions than existing computational methods.

4.3.5 Confidence Interval Analysis

The confidence interval analysis based on 95% confidence levels was performed in order to examine the reliability and accuracy of the outcomes generated by the proposed approach. The confidence intervals for the prediction accuracy, optimization accuracy and optimization stability scores were computed. It turned out that the uncertainty in predictions made with HCNFF and AQAI-Net remained relatively low because of the narrow width of confidence intervals, which is associated with high prediction accuracy and reliable optimization.

Table 21: Confidence Interval Analysis Table

Framework	Mean Accuracy (%)	Lower Confidence Limit	Upper Confidence Limit
HCNFF	98.88	97.94	99.42
AQAI-Net	98.91	98.02	99.36

The table 21 represents narrow range of confidence intervals implies the high level of statistical reliability, reproducibility and computational stability of the proposed intelligent structures for the applications of environmental nanotechnology and wastewater purification.

5. Discussion

The Discussion chapter describes the strengths and weaknesses of the proposed HCNFF and AQAI-Net taking into consideration their contributions, reproducibility and limitations. It provides the systematic analysis of the impact of each component on the performance of the whole system as well as its stability. Moreover, it emphasizes the reliability and application potential of the proposed approach to environmental nanoparticles.

5.1AblationStudy

The objective of the ablation experiments was to investigate the impact of all the components included in the framework for the HCNFF and AQAI-Net models. Removing the modules responsible for hierarchical feature learning and cognitive weighting and quantum-inspired optimization revealed outstanding performance when considering prediction accuracy and optimization efficiency, respectively. The lack of cognitive feature adaptation resulted in decreased interpretability of the resulting models, while there was an increase in prediction errors, particularly. Also, the absence of the quantum-inspired optimization algorithm resulted in a more time-consuming process of training models, due to low optimization capacity. These outcomes indicate the importance of every component to the general performance of the developed solution.

5.2 Reproducibility and Experimental Reliability

The standardization process in terms of the data pre-processing procedure, the parameters setting process and the training validation procedure of the two algorithms mentioned; i.e., HCNFF and AQAI-Net ensures

very high levels of reproducibility of the results generated through the experiments conducted using these two algorithms. With the same normalization of the data and parameters optimization process, the performances generated will remain the same during several repetitions of the process. Moreover, the results of the statistical validation analysis indicate that there is little deviation from the anticipated result, hence indicating reliability of the experiment.

5.3 Limitations of the Proposed Framework

But despite all the benefits, there are certain limitations of the framework including reliance on the quality and availability of the data that is already existing. Furthermore, the use of hybrid deep learning and quantum optimization techniques within the framework comes with high computational costs as well. Implementation and integration of the framework into practice could prove to be extremely challenging due to its complex nature. There is a need for validating the framework using a larger sample size to ensure increased generalizability of results.

6. Conclusion

The synthesized ZnO-doped Fe_2O_3 nanoparticles exhibited excellent environmental remediation properties with the incorporation of intelligent prediction and optimization frameworks for advanced wastewater treatment applications. The structural characterization analysis confirmed that there was a significant improvement in the properties of the nanoparticles, the crystallite size was reduced to 29.6 nm, the lattice strain was reduced to 0.21% and the surface area was increased to 61.9 m^2/g and the pore volume reached 0.29 cm^3/g, which means it has improved porosity and active surface interaction. The developed nanocomposite showed high efficiency in removing Methylene Blue dye, 97.8% and heavy metal, 97.2%, removal efficiency and proved to be excellent in environmental adaptability and adsorption ability. The proposed HCNFF was found to be superior for the prediction performance with the mean absolute error (MAE) being 0.74, means square error (MSE) 1.62, root mean square error (RMSE) 1.27, maximum prediction accuracy 98.88% and stability score 98.30%. Likewise, the optimization accuracy, convergence speed and automation stability of AQAI-Net were 98.91%, 97.86% and 98.32% respectively. Overall, the proposed work presented a scalable and computational efficient solution to the sustainable environmental nanotechnology applications using an intelligent framework. Large-scale industrial wastewater remediation and real-time environmental monitoring systems in the future works.

Acknowledgement

The authors would like to thank their respective institutions for providing the necessary facilities and support to carry out this research work. The authors declare that the manuscript is original, has not been published previously, and is not under consideration for publication elsewhere.

Statement and Declaration

Funding: The authors declare that no financial support or funding was received for this research work.

Conflict of Interest: The authors declare that they have no known competing financial interests or personal relationships that could have influenced the work reported in this article.

Ethical Approval: This article does not contain any studies involving human participants or animals performed by any of the authors.

Data Availability Statement: N/A

Author Contributions: All authors contributed equally to the conception, experimental work, analysis, and preparation of the manuscript. All authors reviewed and approved the final version of the manuscript.

References

[1] Al-Essa K, Hassanien R, Al-Saydeh R (2025) Advanced nanocomposite catalysts for waste management: Fe_3O_4-doped ZnO for dye degradation via pulsed laser ablation in liquid media. *Arab J Chem* **18**:106204. https://doi.org/10.25259/AJC_449_2025

[2] Asghari M, Taghvaei V, Hashemi B, Shafiei M, Alipanah L (2025) Biosynthesis of magnetic ZnO@Fe_2O_3 nanocomposites decorated with Ag/AgCl using Hormoz Island's red soil and *Avicennia marina* leaf extract. *Sci Rep* **15**:14892. https://doi.org/10.1038/s41598-025-98442-w

[3] Akbar S, Abid M, Fatima B, Mehmood T, Riaz T, Khurshid M (2024) Green synthesis and characterization of Fe_2O_3, ZnO and TiO_2 nanoparticles and their potential use as biofertilizer on sunflower. *Physiol Mol Biol Plants* **30**:1429–1447. https://doi.org/10.1007/s12298-024-01508-8

[4] Bollinger J-C, Kenfack Tonle I, Njanja E (2026) Green synthesis of ZnO/Fe_2O_3 nanocomposites using *Urtica dioica* extract: Evaluation of photocatalytic, antioxidant and antibacterial activities. *Catalysts* **16**:276. https://doi.org/10.3390/catal16030276

[5] Bouafia A, Laouini SE, Khelef A, Meneceur S, Tedjani ML, Barhoum A (2025) Bio-inspired synthesis and photocatalytic applications of α-Fe_2O_3@ZnO nanobinary using *Laurus nobilis* leaf extract: Efficient for anionic and cationic dye degradation with reusability studies. *Appl Organomet Chem* **39**:e70119. https://doi.org/10.1002/aoc.70119

[6] Gherbi B, Laouini SE, Meneceur S, Bouafia A (2024) Removal of hydrocarbons and heavy metals from petroleum water by modern green nanotechnology methods using α-Fe_2O_3, CuO and ZnO nanoparticles. *Sci Rep* **14**:8142. https://doi.org/10.1038/s41598-023-32938-1

[7] Green F, Jiang Q, Liu S, Zhang Y, Wang R (2024) Co-precipitation synthesis of Zn-doped α-Fe_2O_3 nanoparticles: Structural, optical and dielectric properties. *Ceram Int* **50**:47244–47252. https://doi.org/10.1016/j.ceramint.2024.08.367

[8] Haiouani K, Hegazy S, Alsaeedi H, Bechelany M, Barhoum A (2024) Green synthesis of hexagonal-like ZnO nanoparticles modified with phytochemicals of clove (*Syzygium*

aromaticum) and *Thymus capitatus* extracts: Enhanced antibacterial, antifungal and antioxidant activities. *Materials* **17**:4340. https://doi.org/10.3390/ma17174340

[9] Manojkumar D, Kaliannan D, Balasubramanian B (2024) A novel photocatalytic degradation of mixed dye through chemically synthesized ZnO/Fe_2O_3 nanocomposite. *Environ Geochem Health* **46**:221. https://doi.org/10.1007/s10653-024-02000-8

[10] Qi L, Wang S, Liu Y, Zhao P, Tian J, Zhu B, Zhang S, Xie W, Yu H (2024) Facile preparation of magnetically separable Fe_3O_4/ZnO nanocomposite with enhanced photocatalytic activity for degradation of Rhodamine B. *Nanomaterials* **14**:926. https://doi.org/10.3390/nano14110926

[11] Arenas R, Escobedo A, Romero M (2025) A machine learning approach to determine the band gap energy of high-entropy oxides using UV-Vis spectroscopy: Bagging, Extra Trees and Random Forest algorithms. *Nanomaterials* **6**:340. https://doi.org/10.3390/nano6120340

[12] Feng S, Wang J (2024) Prediction of organic–inorganic hybrid perovskite band gap by multiple machine learning algorithms: XGBoost, Random Forest, LightGBM and GBR. *Molecules* **29**:499. https://doi.org/10.3390/molecules29020499

[13] Ju HA, Thanh Hoang D, Jang WS, Kim YH, Park EB, Lee H (2025) Convolutional neural networks for automatically analyzing morphology and size of nanobiomaterials in electron microscope images. *Colloids Surf B Biointerfaces* **248**:114563. https://doi.org/10.1016/j.colsurfb.2025.114563

[14] Makota O, Dutková E, Briančin J, Bednarcik J, Lisnichuk M, Yevchuk I, Melnyk I (2024) Advanced photodegradation of azo dye methyl orange using H_2O_2-activated Fe_3O_4@SiO_2@ZnO composite under UV treatment. *Molecules* **29**:1190. https://doi.org/10.3390/molecules29061190

[15] Nawaz R, Arshad U, Hanafiah MM, Haider S, Anjum M, Zaini SB (2025) Machine learning approach for photocatalysis: An experimentally validated case study of photocatalytic dye degradation using Cu_2O/WO_3 and ZnO nanoparticles. *J Hazard Mater* **482**:136700. https://doi.org/10.1016/j.jhazmat.2025.136700

[16] Racik KM, Manikandan A, Mahendiran M (2024) α-Fe_2O_3/ZnO nanocomposite as an efficient photocatalyst for wastewater treatment and flexible electronic device applications. *Ionics* **30**:1215–1229. https://doi.org/10.1007/s11581-023-05316-0

[17] Alsaedi SS, Mohammed SS, Mahdi AE, Shnain ZY, Majdi HS, AbdulRazak AA, Alwasiti AA (2024) Machine learning-enhanced band gaps prediction for low-symmetry double and layered perovskites using SVR, RFR, GBR and XGBoost. *Sci Rep* **14**:25884. https://doi.org/10.1038/s41598-024-77081-7

[18] Song C, Shi Y, Li M, He Y, Xiong X, Deng H, Xia D (2024) Application of machine learning models to improve the prediction of pesticide photodegradation in water by ZnO-based photocatalysts. *Chemosphere* **362**:142632. https://doi.org/10.1016/j.chemosphere.2024.142632

[19] Tigabu E, Mulaw G, Ferede E (2025) Green synthesis, characterization, antibacterial and antifungal activity investigation of zinc oxide nanoparticles using *Verbascum sinaiticum* leaf extract. *Inorg Chem Commun* **173**:114248. https://doi.org/10.1016/j.inoche.2025.114248

[20] Yılmaz M, Güneş A, Kaya S, Çelik S (2024) Morphological analysis of Pd/C nanoparticles using SEM imaging and advanced deep learning techniques with attention mechanism. *RSC Adv* **14**:34951–34962. https://doi.org/10.1039/D4RA06113F

[21] Halawa OM, Ahmed E, Abdelrazek MM, Nagy YM, Abdelraouf OA (2026) Recent progress in nanophotonics for green energy, medicine, healthcare and optical computing applications. *Materials* **19**:1660. https://doi.org/10.3390/ma19081660

[22] Kakhki RM, YereyehZadeh F, Mohammadpoor M (2025) Precision photocatalysis: Machine learning driven parameter optimization for S-doped ZnO/chitosan tetracycline degradation. *Research Square* (Preprint). https://doi.org/10.21203/rs.3.rs-6841423/v1

[23] Khamkure S, Treesatayapun C, Bustos-Terrones V, Díaz Jiménez L, Pacheco-Catalán D-E, Reyes-Rosas A, Gamero-Melo P, Zermeño-González A, Tippayawong N, Pholchan P (2026) A fuzzy-driven synthesis: MiFREN-optimized magnetic biochar nanocomposite from agricultural waste for sustainable arsenic water remediation. *Technologies* **14**:43. https://doi.org/10.3390/technologies14010043

[24] Konstantopoulos G, Koumoulos EP, Charitidis CA (2022) Digital innovation enabled nanomaterial manufacturing: Machine learning strategies and green perspectives. *Nanomaterials* **12**:2646. https://doi.org/10.3390/nano12152646

[25] Liang X, Yu S, Meng B, Ju Y, Wang S, Wang Y (2025) Machine-learning-guided design of nanostructured metal oxide photoanodes for photoelectrochemical water splitting: From material discovery to performance optimization. *Nanomaterials* **15**:948. https://doi.org/10.3390/nano15120948

[26] Rehman A, Iqbal MA, Haider MT, Majeed A (2025) Artificial intelligence-guided supervised learning models for photocatalysis in wastewater treatment. *AI* **6**:258. https://doi.org/10.3390/ai6100258

[27] Sheikhmohammadi A, Alamgholiloo H, Golaki M, et al. (2024) Cefixime removal via WO_3/Co-ZIF nanocomposite using machine learning methods. *Sci Rep* **14**:13840. https://doi.org/10.1038/s41598-024-64790-2

[28] Sheikhmohammadi A, Hosseinpour S, Jalilzadeh Z, et al. (2025) Harnessing AI to revolutionize photocatalytic degradation of tetracycline via optimized UV/ZrO_2/NaOCl reaction pathways. *Sci Rep* **15**:18852. https://doi.org/10.1038/s41598-025-03814-x

[29] Zainulabdeen S, Haifaa NB, Atiyah IA (2025) An advanced multi-branch recurrent deep learning model for predicting the antibacterial capacity of nanoparticles with SHAP-based explainability. *Muthanna Med J* **12**:13–28. https://muthmj.mu.edu.iq/journal/vol12/iss3/2/

[30] Zhu C, Samuel OD, Taheri-Garavand A, et al. (2025) ANN-ANFIS model for optimising methylic composite biodiesel from neem and castor oil and predicting emissions of the biodiesel blend. *Sci Rep* **15**:5638. https://doi.org/10.1038/s41598-025-88901-9